

INVESTIGATION INTO THE EFFECT OF DIRECTIONALITY ON MECHANICAL PROPERTIES OF HIGH STRENGTH STEEL

A DISSERTATION

*submitted in partial fulfilment of the
requirements for the award of the degree*

of

MASTER OF ENGINEERING

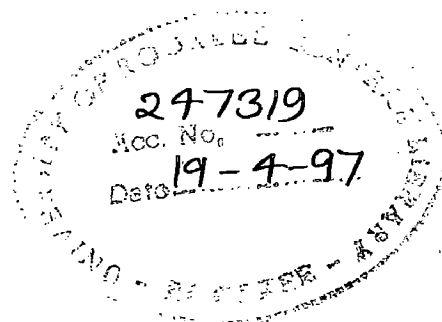
in

MECHANICAL ENGINEERING

(With Specialization in Welding Engineering)

By

ALAMGEER ABEDEEN



DEPARTMENT OF MECHANICAL AND INDUSTRIAL ENGINEERING
UNIVERSITY OF ROORKEE
ROORKEE-247 667 (INDIA)

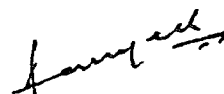
MARCH, 1996

CANDIDATE'S DECLARATION


I hereby declare that the work which is being presented in this dissertation entitled "INVESTIGATION INTO THE EFFECT OF DIRECTIONALITY ON MECHANICAL PROPERTIES OF HIGH STRENGTH STEEL" in partial fulfilment of the requirements for the award of the degree of "Master of Engineering" in Mechanical Engineering (With specialization in Welding Engineering) submitted in Mechanical and Industrial Engineering Department, University of Roorkee, Roorkee is an authentic record of my own work, carried out from July 1995 to March 1996, under the supervision of Mr. Ajai Agarwal, *Lecturer*, Mechanical and Industrial Engineering Department, and Dr. Satya Prakash, *Professor*, Department of Metallurgical Engineering, University of Roorkee, Roorkee.

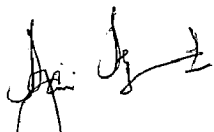
The matter embodied in this dissertation has not been submitted by me for award of any other degree.

Dated: 30th March, 1996


(ALAMGEER ABEDEEN)

This is to certify that the above statement made by the candidate is correct to the best of our knowledge.


(Dr. Satya Prakash)
Professor
Department of Metallurgical Engg.
University of Roorkee
Roorkee- 247 667 (India)


(Mr. Ajai Agarwal)
Lecturer
Mechanical & Ind. Engg.
Department
University of Roorkee
Roorkee-247 667 (India)

ACKNOWLEDGEMENT

The present work is an outcome of towering guidance throughout the course of investigation, by my guides, Mr. Ajai Agarwal, *Lecturer*, Mechanical and Industrial Engineering Department, and Dr. Satya Prakash, *Professor*, Department of Metallurgical Engineering, University of Roorkee, Roorkee. I found myself deserted of words to acknowledge my gratefulness for their unparalleled efforts and perpetual help .

I can not escape expressing my indebtedness to Dr. P.C. Gupta, Professor, Mechanical & Industrial Engineering Department, University of Roorkee, Roorkee without his active co-operation and suggestions, this dissertation work would not have seen the light of the day.

I wish to thank all my friends who directly or indirectly helped me. Finally my thanks are also extended to staff of 'Welding Research Laboratory' for their co-operation and generous support.

Dated: 30th March, 1996


(ALAMGEER ABEDEEN)

ABSTRACT

In the present work, the conventional and fracture mechanics properties, mainly, cyclic crack growth rate is assessed in longitudinal, transverse & short-transverse directions in order to find out the effect created by directionality on the various properties of a high strength steel. The various tests which have been done include hardness, tensile, charpy and fracture mechanic tests. It has been found that microstructure is same in the longitudinal and the transverse directions and varies in the short transverse direction. In the case of hardness, leaving the longitudinal direction there was variation in the other two directions. The tensile strength was highest in the transverse direction whereas the charpy values were lowest in this direction finally crack-growth was lowest in the short transverse direction.

CONTENTS

	Page No.
CANDIDATE'S DECLARATION	i
ACKNOWLEDGEMENT	ii
ABSTRACT	iii
LIST OF FIGURES	iv
LIST OF TABLES	vi
CHAPTER-ONE	
INTRODUCTION	1
CHAPTER-TWO	
LITERATURE REVIEW	2
2.1 Anisotropy	2
2.2 High Strength Steels	5
2.3 Rail Steels	6
2.4 Rail Road-Rail Production	6
2.4.1 Heat treatment and alloying of rails	7
2.4.2 Major types of defects and failure of rails	8
2.5 Brittle Fracture and Transition Temperature	9
2.6 Fatigue	11
2.6.1 Parameter affecting fatigue strength	14
2.6.2 Fatigue crack initiating and near-threshold crack	15
2.6.3 Macro-fatigue-crack-growth	16
2.6.4 Influence of microstructure on fatigue	17
2.6.5 Micro-mechanisms of cleavage fracture in rails	17

2.7	Toughness	17
2.7.1	Notch toughness	18
2.7.1.1	Factors affecting notch toughness	18
2.7.1.2	Use of notch toughness	18
2.7.2	Fracture toughness	19
2.8	Fracture Mechanics	19
2.9	Application of Fracture Mechanics	23
2.9.1	Fatigue life	24
2.9.2	Fatigue-crack-growth-rate	24
2.9.2.1	Factors affecting fatigue-crack-growth-rate	26
2.9.2.2	Correlation between fatigue-crack-growth-rate and microstructural variables in rail steel.	27
2.10	Testing Standards	28
2.10.1	ASTM E 8-86	28
2.10.2	ASTM E 23-86	29
2.10.3	ASTM E 647-86 a	30
2.11	Mechanical Properties Assessment	31

CHAPTER-THREE

EXPERIMENTAL PROCEDURE	32	
3.1	Materials	32
3.2	Microstructural studies	32
3.3	Hardness tests	32
3.4	Tensile tests	33
3.5	Impact tests	33
3.6	Fatigue crack growth rate (FCGR) tests	34

CHAPTER-FOUR

RESULTS AND DISCUSSION	36
4.1 Results	36
4.1.1 Chemical composition	36
4.1.2 Microstructure	36
4.1.3 Hardness tests	36
4.1.4 Tensile tests	37
4.1.5 Impact tests	37
4.1.6 Fatigue crack growth rate (FCGR) tests	38
4.2 Discussion	38
4.2.1 Microstructure	38
4.2.2 Hardness tests	38
4.2.3 Tensile tests	39
4.2.4 Impact tests	39
4.2.5 Fatigue crack growth rate (FCGR) tests	40

CHAPTER-FIVE

CONCLUSION	41
-------------------	-----------

CHAPTER-SIX

SCOPE OF FUTURE WORK	43
-----------------------------	-----------

REFERENCES	44
-------------------	-----------

LIST OF FIGURES

Fig.No.	Title	Page No.
2.1	Effect of grain size on toughness	47
2.2	Direction of crack growth in rolled plate.	47
2.3	Effect of the ferrite grain size on the impact transition temperature and yield strength of 0.1% C steel.	47
2.4	Schematic variation of fracture stress (σ_f) and yield stress (σ_y) with temperature for steel.	48
2.5	Plot between No. of cycles to failure and stress amplitude (i.e., N_f Y_s σ_a)	49
2.6	Plot N_f Vs σ_a showing effect of notch.	49
2.7	Plot showing effect of mean stress on σ_e .	49
2.8	Plot showing effect of temperature on σ_u .	50
2.9	Plot showing effect of corrosive environment on σ_e .	50
2.10	Plot showing effect of size on σ_e .	50
2.11	Model for equations for stresses at a point near a crack.	51
2.12	Effect of fatigue crack growth on S-N curve.	51
2.13	Schematic variation of fatigue crack growth rates (da/aN) with alternative stress intensity range (4K).	52
2.14	Variation of fatigue crack growth rates (FCGR) with K_{Ic} .	52
3.1	Location of specimen for transverse and microstructural studies.	53
3.2	Drawing of the tensile specimen.	54

3.3	Location of tensile test specimen in the rail section.	55
3.4	Drawing of impact specimen.	55
3.5	Location of the impact specimen in rail section.	56
3.6	Drawing of C.T. specimen.	54
3.7	Location of the C.T. specimen in the rail section.	57
4.1 a :	Micrographs of longitudinal specimen.	58
4.1 b :	Micrographs of transverse specimen.	59
4.1 c :	Micrographs of short-transverse specimen.	60
4.2	Stress Vs Strain curve of longitudinal specimen (1a).	61
4.3	Stress Vs Strain curve of longitudinal specimen (2a).	62
4.4	Stress Vs Strain curve of longitudinal specimen (3a).	63
4.5	Stress Vs Strain curve of short-transverse specimen (2c).	64
4.6	Stress Vs Strain curve of short-transverse specimen (3c).	65
4.7	Stress Vs Strain curve of transverse specimen (1b).	66
4.8	Stress Vs Strain curve of transverse specimen (2b).	67
4.9	Stress Vs Strain curve of transverse specimen (3b).	68
4.10	Log da/dN Vs log (ΔK) curve of specimen - 1.	69
4.11	Log da/dN Vs log (ΔK) curve of specimen - 2.	70

LIST OF TABLES

Table No.	Title	Page No.
2.1	American Society for Testing and Materials High-Strength Low Alloy Structural Steel. A 242-63T	71
2.2	American Society for Testing and Materials High-Strength Structural Steel. A 440-59T	72
2.3	American Society for Testing and Materials High-Strength Low Alloy Structural manganese-vanadium steel. A 441-60T	73
2.4	Chronological Development of Heat Treatment and Alloying of rails.	74
2.5	Major Types of rail defects and failure of rails.	75
4.1	Chemical composition of medium manganese rails and head hardened rails.	76
4.2	Results of macro-hardness tests.	76
4.3	Results of micro-hardness tests.	77
4.4	Results of tensile tests.	78
4.5	Results of impact tests.	79
4.6	Fatigue crack growth rate (FCGR) test results of specimen-1.	80
4.7	Fatigue crack growth rate (FCGR) test results of specimen-2.	81

INTRODUCTION

Mechanical fibering is of importance for all kinds of materials. It is the main cause of differences in strength, ductility and toughness found from specimens oriented parallel and transverse to the direction of metal flow during processing. In a material having a degree of alignment of inclusions, stresses interact with aligned inclusions, leading to anisotropy in properties related to the fracture behaviour of the material. The term inclusion is used in the general sense to denote all types of fracture nuclei such as pores, chemically segregated areas, second phase particles, foreign inclusion etc.

Highest toughness is usually found in the specimens oriented in the longitudinal direction with the crack propagation in the short transverse direction, and lowest toughness in the specimens oriented in the short-transverse direction with the crack propagation in the transverse or longitudinal direction. Approximately 50% improvement is obtained by aligning the specimen in the longitudinal direction and crack propagation in the short-transverse direction. This anisotropic effect can be utilised in designing of the structure and correlating the properties in different directions in order to assess the life span in advance.

LITERATURE REVIEW

2.1 Anisotropy

Anisotropy is the characteristic of exhibiting different values of a property in different directions with respect to a fixed reference system in the material. Material is always more or less anisotropic and heterogeneous in strength due to previous manufacturing processes (e.g., rolling, heat-treatment, etc). Toughness and ductility of engineering materials are sensitive to processing variables [1]. A given alloy has no unique toughness, but a whole range of values corresponding to different processing histories, each resulting in minor variations in microstructure. Each processing step can have an effect on toughness.

A structural variable that is affected by processing is the grain size. Theoretical considerations by Hall and Petch show the mechanical properties of steel to be inversely proportional to the square root of the grain size. By using this relationship, Ensha and Tetelman [1] have derived an equation giving the dependence of fracture toughness on grain size. They found good agreement with a limited set of data (Fig. 2.1).

In general the processing steps causing changes in yield strength and ductility will also affect the toughness of a material, as a result of the direct relation between these properties. The effect of processing on toughness

can become particularly troublesome when it causes non-uniformity or structural inhomogeneities, due to unavoidable variations of the processing histories within the material. Inclusions are, of course, oriented by the rolling that occurs during the steel production process and thus contribute to fatigue anisotropy (The term "inclusion" is used in the general sense to denote all types of fracture nuclei such as weak interfaces, pores, chemically segregated areas, second phase particles, foreign inclusions, etc.). In parts of complicated geometry the cooling rates may vary considerably from point to point despite many corrective measures. Segregation in ingots may persist through further processing, and local structural changes may occur due to machining and cold work.

Deformation of materials produces an anisotropy. A mechanical anisotropy with respect to toughness exists in all wrought products forgings as well as rolled material. Hot or cold deformation may lead to the alignment of crystallographic axes of the grains into a preferred orientation or texture. It also causes mechanical fibering: elongated grains and strings or bands of elongated inclusions and second phase particles. Finally, the processing may introduce residual stresses.

Anisotropy due to crystallographic texture is of special importance for cleavage fracture, since cleavage takes place along preferred crystallographic planes. There may be a lower resistance to cleavage when the cleavage planes of neighbouring grains are aligned. Mechanical fibering is of importance for all kinds of materials. It is the main cause of differences in strength, ductility and toughness found from specimens oriented parallel and transverse to the direction of metal flow during processing. A number of investigations have pointed out that K_{IC} is very sensitive to test piece orientation in the parent

material. The development of preferred orientations and 'banding' due to metal-forming operations means that a crack finds more difficulty propagating normal rather than parallel to the fibre direction and the fracture toughness is thus superior in the former instance. The various possibilities for crack propagation in rolled stock are depicted in Fig. 2.2. Specimens oriented in the short transverse direction (crack growth in longitudinal or transverse) show especially low toughness.

The variations in toughness for various directions of crack propagation can be very large. For an 18% nickel maraging steel, the toughness of longitudinal specimens (spec. 3 in Fig. 2.2) has been reported to be twice as high as the toughness of short-transverse specimens (spec. 5). For an aluminum-zinc-magnesium alloy, fracture toughness values of $126 \text{ kg/mm}^{3/2}$, $67 \text{ kg/mm}^{3/2}$ and $53 \text{ kg/mm}^{3/2}$ have been reported for the longitudinal, transverse, and short-transverse directions, respectively. Ransom found transverse/longitudinal fatigue-limit ratio of 0.52 in a 0.36% carbon steel heat treated to HRC 28. In another steel (27 HRC), which was somewhat cleaner, he found a ratio of 0.68. Stulen, Cumming and Schulte recommend taking anisotropy into account when designing against fatigue, even though properties other than longitudinal are not generally available. They recommend that properties in oblique directions to be decreased by 20 to 30% [2].

The fracture plane, following the grain flow, is the plane of lowest crack resistance. The directional effect on K_{IC} is of importance for the residual strength in the case of semi-elliptical surface flaws and quarter elliptical corner cracks in rolled material. It is one of the reasons why specimens with elliptical cracks do not show consistent K_{IC} values. So, the stress intensity at fracture will depend upon flaw shape, and surface. Flaw specimens will generate

apparent fracture toughness data which depend upon flaw shape. Or, in other words K_{IC} of a surface flaw specimen depends upon flaw shape. There are important factors to be considered in anisotropic behaviour.

- (i) The effect will be aggravated by high contents of slow diffusing alloys, i.e., in high-alloy steels.
- (ii) The relation of preferred orientation to service stresses may be extremely important.
- (iii) It is rarely possible to obtain valid K_{IC} data for all the desired test piece/work-piece orientation.

2.2 High Strength Steels

High Strength steels are classified as [3], [4]

ASTM spec A242 : High strength low alloy structural steel

ASTM spec A440 : High strength structural steel for non-welded fabrication.

ASTM spec A441 : High strength structural steel for welded fabrication.

In the period between 1900 and 1940 many proprietary grades of steel were supplied primarily for high strength structural specifications in bridges. In 1941 an attempt was made to include these high-strength steels in comprehensive specification A242, "High-strength Low-Alloy Structural Steel", shown in Table-2.1 .

Since control of specific alloy addition was left to the discretion of the manufacturer, confusion arose as to which grades of A242 were weldable. This was finally resolved in 1959 by the adoption of high-strength steel specification A440 for non-welded fabrication and A441 for welded fabrication, shown respectively in Tables-2.2 & -2.3 .

2.3 Rail Steels

Steels which have predominantly pearlitic structures are widely used for such purposes as rails, wheels, axles, etc, in railway engineering [5]. The increased pearlitic content plays a useful role in increasing the tensile strength and imparting a measure of wear resistance, but at the expense of a deleterious effect on the impact toughness and overall ductility. Traditionally these steels have not been required to possess a large measure of toughness but recent failures have highlighted the need for improved toughness. This could be achieved by lowering the carbon content, but only at the expense of introducing ferrite into the structure with a resulting loss of strength and wear resistance. Consequently, systematic investigations into the factors controlling the strength and toughness have led to a more complete understanding of the way in which the properties may be optimized. The general composition of rail steel is

C : 0.6 - 0.80%

Mn : 0.6 - 1.00%

P(max): 0.04%

Si : 0.1 - 0.23%

2.4 Railroad-Rail Production

Exposed to weather at all times, railroad-rail is subjected, under constantly varying conditions, to high compression and bending stresses, impact, vibration, friction and wear [6]. Rails are formed by three general methods of rolling:

1. The tongue-and-groove, flat or slab-and-edging method;
2. The diagonal or angular method; and
3. The universal method.

The universal rolling method allows a greater degree of hot working of the head and flange of a rail by compression than can be obtained when horizontal rolls alone are used. The final shape, which the rails achieve, is obtained after undergoing 13 passes under hot rolls.

Rails must be free of shatter cracks caused by hydrogen. To accomplish this, hydrogen must be eliminated by vacuum treatment of the steel or by controlled cooling of rails, or blooms.

2.4.1 Heat-Treatment and Alloying

The important rail processing techniques used for the improvement of mechanical properties are summarised in Table-2.4. The mechanical properties are achieved by obtaining the optimal metallurgical structures.

Some investigators [7], [8] obtained pearlitic structure of very fine lamellae spacings by resorting to different heat treatment practices. The second method involves alloying the standard carbon-manganese rail steels [7] using different alloying elements. But this route is considered expensive due to expensive alloy additions and low productivity rates. Others have used the accelerated cooling of the rail as it leaves the hot rolling mill. Even after introducing the cooling by steam and hot water, it was difficult to achieve critical cooling rates to have consistency in operation. Variation of temperature upto $\pm 50^{\circ}\text{C}$ was most common along the length of the rail.

Recently, an improved process for head hardening of rails in line with production rolling has been developed [9]. The head only of the rail is heat treated from end to end by passing the rail lengthwise through an induction coil, shaped like an inverted U to heat the head to austenitizing temperature. Heating is followed by an air quench. The air-quenched portion is tempered by residual heat in the rail. A special prebend and subsequent final water-cooling results in a straight rail after treatment. Rail heads are hardened to between 321 and 388 Brinell hardness. Very fine pearlitic microstructures with good weldability and wear resistance is the main feature of this process [6].

2.4.2 Major Types of Defects and Failure of Rails

In rail-road industries, rail defects are classified as material defect and service defect. The former originates during processing while the latter originates during actual service period.

The important defects, their causes and remedies are summarised in Table-2.5. Hydrogen induced shatter cracks are most common in pearlitic rail steels [10], whose susceptibility are enhanced by higher hydrogen and Mn to C ratio and reduced by higher sulphur content. Shelling classified as horizontal crack in service is caused due to soft rails and heavy loads. Shells are formed after plastic deformation. Harder rails are less prone to shelling.

Other important fractures in rails are transverse fissure, showing rapid growth, progressive fracture due to compound fissure, welded burn fracture initiated at an engine burn and star cracking at fish bolt.

By introducing the efficient steel processing techniques such as continuous casting process, low hydrogen steel melting and, the improved cleanliness of

steel, rail defects like shatter cracks, transverse fissures, progressive fracture are minimised to a considerable extent. The control of microstructure through alloying and heat treatment have increased the resistance to unstable cleavage fracture.

2.5 Brittle Fracture and Transition temperature

Brittle fracture and fatigue failure are inseparable. The ultimate mechanism of brittle fracture is usually regarded as a simple elastic extension of atomic bonds upto the point of final separation. These cleavage failure are associated with very little or negligible plastic deformation and occurs in steels at low temperatures. The propagation of such a cleavage crack requires much less energy than that associated with the growth of a ductile crack as can be easily illustrated by measuring the absorbed energy in an impact test such as the charpy test. In order for brittle failures to occur in practice a defect or notch of some sort is usually required together with a tensile stress. This also requires the temperature level to be critical.

As the mode of fracture changes from brittle to ductile, there is often a marked change with temperature leading to the concept of ductile-brittle transition temperature. However it must be emphasized that there is a widespread scatter in tests like charpy with most commercial steels and the transition more usually occurs over a range of temperature. More over the transition temperature is not fixed, and it is quantified by various criteria like Nil-ductility transition temperature (NDTT), Fracture transition plastic (FTP) criyeria, etc., and it changes as the specimen size and rate of straining are modified [11]. Transition temperature is an arbitrarily defined temperature within the

temperature range in which metal fracture characteristics determined usually by notched tests are changing rapidly such as from primarily fibrous (shear) to primarily crystalline (cleavage) fracture. Commonly used definitions are "transition temperature for 50% cleavage fracture", "10-ft-lb transition temperature", and "Nil ductility transition temperature" [12].

All the body centered cubic materials show a marked dependence of the yield stress on temperature due to the variation of the Peirls-nebarro stress (the stress to move dislocations through the microstructure) with temperature. As the temperature is lowered below the room temperature, the yield stress is increased and the first dislocation to move, will do so rapidly, as the velocity is proportional to the stress [11]. It is well known that the ductile-brittle transition temperature can be reduced by refining the grain size and this technique is commonly used in practice to produce improved materials (Fig. 2.3). If the cracks are formed by dislocations piling up at the grain boundaries, then smaller the grain size, the smaller will be the dislocation pile-up length, the resulting local stress concentration and the number of microcracks [13].

An examination of Fig. 2.4(a) shows that both σ_f (tensile stress for crack propagations or fracture stress) and σ_y (yield stress) in general increases with decreasing temperature with σ_y showing the greatest effect. At relatively high temperatures, the material yields microscopically prior to fracture whereas at low temperatures the material is completely brittle. At the transition temperature, T_C the yield and fracture stress are coincident. According to Hall-Petch Heslop equation,

$$\sigma_y = \sigma_i + Kd^{-1/2} \quad 2.1$$

where ,

σ_y = Lower yield strength

σ_i = Lattice friction stress

k = material constant

d = grain dia

This equation explains the linear relationship between T_c & $d^{-1/2}$. Any feature which increases the yield strength, other than grain refinement, causes an increase in σ_i and a resulting increase in the transition temperature as indicated by Fig. 2.4(b). Thus solid solution strengthening, precipitation hardening and work hardening all raise the transition temperature. On the other hand, reducing the fracture stress by introducing notches in the test piece, results in an increase in the transition temperature as shown in Fig. 2.4(c). Examination of the equation controlling fracture and yielding behaviour indicates that grain refinement results in an increase in both σ_f and σ_y , although it has a greater effect on σ_f than on σ_y as shown in Fig. 2.4(d). The net effect is to move the fracture transition to lower temperatures. In comparison with other methods of increasing strength, grain refinement is the only one which enables strength and toughness to be increased simultaneously and for this reason, it is the one that is widely used in practice [11].

2.6 Fatigue

It is defined as the cumulative damage caused to the material (or component) by cyclic or fluctuating loading. The first systematic study on fatigue was conducted by a German Engineer "Wohler" in 1860 while working on the failure of railway axles [14]. He found if load is cyclic i.e., load is a

function of time, then at various loads, the failure occurs after the component undergo a no of cycles.

Plotting $N_f V_s \sigma_a$, (Fig. 2.5),

where,

N_f = no of cycles to fail and

σ_a = stress amplitude,

he found that at a particular stress amplitude the no. of cycles required to failure is practically infinite, which in turn is called 'fatigue limit' or 'Endurance limit' of the material.

Fatigue strength is seriously reduced by introduction of a stress raiser such as a notch or a hole. The effectiveness of a notch in decreasing the fatigue limit is expressed by the fatigue strength reduction factor or fatigue notch factor, K_f . The value of K_f is found to vary with

- (i) the severity of the notch
- (ii) the type of the notch
- (iii) the material
- (iv) the type of loading, and
- (v) the stress level.

K_f is usually less than K_t , and is defined as

$$K_f = \frac{\text{fatigue strength of un-notched component}}{\text{fatigue strength of notched component}}$$

K_f is given by

$$K_f = q(K_t - 1) + 1 \quad 2.2$$

where,

K_f - Fatigue strength reduction factor

K_t - Stress concentration factor

where $K_t > 1$.

q - Notch sensitivity factor

where $0 \leq q \leq 1$, and it depends upon the type of material .

$q = 0.75 \sim 0.95$ for high strength materials

$= 0.6 \sim 0.7$ for medium strength materials

$= 0.4 \sim 0.6$ for low strength materials.

There are two types of fatigue (Fig. 2.5).

- (i) Low cycle fatigue (L.C.F): This corresponds to region-A, where fracture stresses are above the yield point of material, i.e., $\sigma_a \geq \sigma_{yield}$ and therefore $\epsilon_{(strain)} > \epsilon_{y(stress \text{ at } yield)}$. Therefore some plastic deformation takes place with each load cycle and the behaviour of material is 'strain-controlled', i.e., fracture is under 'Elastic-Plastic Range' or 'Over Elastic Range'. So material selection becomes critical and a ductile material is preferred in L.C.F and operational conditions play an important role. The no. of cycles required to fracture are very low ($< 10^3$ cycles)
- (ii) High cycle fatigue (H.C.F.): This corresponds to region-B, where all the stresses acting are below the yield stress, i.e. $\sigma_a < \sigma_y$. So the material undergoes the stresses in the Linear Elastic Range and failure is brittle without any deformation. The no. of cycles to fracture is generally more than 10^3 cycles, and materials toughness plays no role in H.C.F. failure. The failure is 'stress-governed' because in Linear Elastic Range only stresses govern the material behaviour.

2.6.1 Parameters affecting Fatigue Strength

(a) Material

$$\sigma_e = f(\text{Material type, Ultimate strength})$$

A brittle material has high endurance limit and ductile material has a low endurance limit. Also $\sigma_e \propto \sigma_u$, i.e. σ_e increases as ultimate tensile strength of the material increases.

(b) Notch Effect (Fig. 2.6)

From eqn. 2.2, we can infer that K_f increases as K_t increases or q increases. So, σ_e decreases as K_t increases or q increases as fatigue strength is inversely proportional to fatigue strength reduction factor.

(c) Mean Stress (Fig. 2.7)

One important effect of mean stress is that positive or tensile mean stress decreases the endurance limit while negative or compressive mean stress increases the endurance limit.

This important effects leads to two results

- (i) Fatigue strength of a material or component can be increased by producing compressive stresses into it
- (ii) Fatigue cracks can be repaired by producing compressive stresses around the crack tip.

(d) *Environment*

Environment = f (Temperature, Corrosion)

(i) *Temperature (Fig. 2.8)*

$$\sigma_e = f(\sigma_u) \text{ and } \sigma_u = f(\text{temperature})$$

$$\text{So, } \sigma_e = f(\text{temperature})$$

As temperature increases, σ_u decreases . So, σ_e also decreases.

(ii) *Corrosive environment (Fig. 2.9)*

σ_e tends to zero under corrosive environment.

(e) *Size effect (Fig. 2.10)*

σ_e decreases as size increases because chances of flaw present increases and gives rise to plane-strain conditions.

2.6.2 Fatigue-crack-initiation and Near-threshold crack Growth

During the process of a fatigue failure, micro-cracks initially form and then coalesce or grow to macrocracks, which propagate until the fracture toughness of the material is exceeded and final fracture occurs. A microcrack may be defined as smaller than a few grain diameters, and a macrocrack may be taken as larger than this. In almost all fatigue failures most of the life time is spent in the initiation and slow growth stages [2].

Fatigue-crack-initiation: Under usual loading conditions, fatigue cracks are known to initiate at or near singularities on or just below the surfaces of metals. Such singularities may be inclusions, embrittled grain boundaries, sharp scratches, pits or slip bands. If the alternating stress amplitude is sufficiently high, slip bands form. These lead to slip steps on the surface, intrusions, extrusions, hills, valleys, ridges or grooves, which in turn lead to initiation of small microcracks. Stress raisers, notches and scratches, of course, hasten initiation by increasing the local stress amplitude. The slip bands may be solely responsible for initiating the crack, or they may interact with geometric defects, such as pits, or with brittle second-phase particles.

Microcrack propagation: A number of factors may act to reduce the growth rate of already-formed microcracks. Crack closure may reduce the rate of crack growth. Microcracks also slow down when they reach the vicinity of neighbouring cracks. A major effect in slowing down microcracks is their interaction with grain boundaries [15].

2.6.3 Macro-Fatigue-Crack Growth

Under cyclic loading, once the microcracks have grown beyond the order of a grain dimensions or so, a "fatal" macrocrack is formed by the continued propagation of a single microcrack or more generally, by the coalescence of several adjacent microcracks. Normally in each stress cycle, a fatigue crack presumably grows in length by an increment and that it does not wait for a number of cycles to pass before each incremental advance [2].

2.6.4 Influence of microstructure on Fatigue

Resistance to microcrack initiation in smooth specimens or ahead of polished blunt notches is clearly increased by utilizing structures of higher strength and finer grain size [2]. Microcrack growth is an intermediate case between fatigue-crack initiation and slow macro-crack propagation. For resistance to micro-crack growth, fine grain size, provided the grain boundaries are not highly embrittled, is an advantage. The grain boundaries stop micro-cracks. Resistance to macro-crack propagation, on the other hand, is decreased in high-strength and (sometimes) finer grain structures.

2.6.5 Micromechanisms of cleavage fracture in rails

In fully pearlitic steels, grain boundary carbides and discrete carbide particles are absent. Park and Bernstein [16] have proposed that cleavage fracture in fully pearlitic steels is propagation controlled. They suggested that crack nucleation is caused by dislocation pile-ups in the ferrite, which impinge on the cementite lamellae and make them to crack. The cracks formed in the cementite lamellae link up and act as a Griffith type of crack which initiates cleavage.

2.7 Toughness

Toughness is the capacity of a material to absorb energy by deforming plastically before fracture [17]. Toughness is determined by the combined strength and ductility of a material and usually is measured by the amount of

work absorbed during the propagation of a crack through a structural member or a standard specimen. The more generally accepted meaning of toughness is resistance to rapid crack propagation, or the absence of brittleness.

2.7.1 Notch Toughness

It is usually evaluated by testing prescribed notched bar specimens at known temperature in a single blow pendulum-type impact machine. The Charpy V-notch impact test is generally considered the preferred method for measuring the notch toughness of steel as it is reliable and reproducible. It can talk about the transition temperature of the material.

2.7.1.1 Factors affecting Notch Toughness

It is characterised into chemical and physical factors.

Chemical Factors: Alloying elements, gas content and impurities.

Physical factors: Hardness, microstructure, homogeneity, grain size, section size, rolling direction, hot and cold working temperatures, method of fabrication and surface conditions (like Carburisation or Decarburisation).

2.7.1.2 Use of notch toughness

- (a) Only useful in design for particular type of structure in a particular kind of service. Can't be used directly for design consideration because it is

dependent on specimen shape & size and service conditions

- (b) Steels with higher transition temperatures can be tolerated when maximum shear stress approaches maximum principal tensile stress.
- (c) When stress concentration and rate of strain are high and service temperatures are low, steels having low transition temperatures must be selected.

2.7.2 Fracture Toughness

It is a measure of toughness, which is independent of specimen shape and size & dependent on material [18], [22]. It is defined as the ability of metal containing an existing small crack or other stress raiser to resist fracture while being loaded under conditions that are unfavourable for energy absorption & plastic deformation. So it is a property of a material which defines its resistance to brittle fracture quantitatively [19], [20].

2.8 Fracture Mechanics

It provides a quantitative framework for evaluating structural reliability in terms of applied stress, crack length, and stress intensity at the crack tip [17], [19]. The linear elastic fracture-mechanics (LEFM) approach to fracture mechanics includes three major assumptions:-

- (i) Cracks and similar flaws are inherently present in parts or specimens.
- (ii) A crack is a flat, internal free surface in a linear elastic-stress field-
purely elastic stress field in an isotropic continuum (featureless solid).

(iii) The quantity of stored energy released from a cracking specimen or part during rapid crack propagation is a basic material property, independent of specimen or part size.

Many failure analysis have confirmed the validity of the first assumption. Cracks are often present in sizes below the limit of sensitivity of non-destructive inspection tests. The second assumption is important for mathematical analysis of stress in the vicinity of crack tip.

LEFM approach [21] is valid when plastic zone is small (as in high strength material), but as plastic zone becomes big we use GYFM (General Yielding Fracture Mechanics) approach. This is the case for low strength material. In ultra-high strength material, both the approaches are valid.

Analysis of crack propagation in brittle material is an important part of fracture mechanics [23]. The idea of fracture mechanics itself was first introduced by Griffith. He analysed the crack extension problem in terms of energy balance of the system which contains the crack.

$$\frac{\partial}{\partial a} (w - \Gamma) = 0 \quad 2.3$$

where,

$2a$ = crack length,

W = the potential energy decrease of the system (the release of stored elastic energy and work done by movement of the external loads), and $\Gamma = 2\gamma a$, the energy of the surface of the crack in which γ is the surface tension of the material.

So, Griffith showed that a crack would propagate if the increase in surface energy generated by crack growth was less than the resulting decrease in elastic energy, i.e., only if the total energy decreased would the crack extend spontaneously under the applied stress.

In order to propagate,

$$\sigma_f = \left[\frac{2\gamma E}{a} \right]^{1/2} \quad 2.4$$

where,

γ = surface tension of the material

$2a$ = crack length

E = Young's modulus

As the crack propagates, the stress needed drops and therefore the crack accelerates and crack propagation is extremely rapid. Griffith's theory has some limitations [24]. It is applicable to linear, elastic and brittle materials and the prediction based on this theory for most engineering materials gives unsatisfactory results. More over the theory ignore the consideration of stresses and strain near the crack tip.

Another approach to fracture mechanics was attempted by Irwin [25]. He examined the stress field near the crack tip. Stress distributions at a point near the crack tip (Fig. 2.11), is given by

$$\sigma_x = \sigma \left(\frac{a}{2r} \right)^{1/2} \left[\cos \frac{\theta}{2} \left(1 - \sin \frac{\theta}{2} \cdot \sin \frac{3\theta}{2} \right) \right] \quad 2.5$$

$$\sigma_y = \sigma \left(\frac{a}{2r} \right)^{1/2} \left[\cos \frac{\theta}{2} \left(1 + \sin \frac{\theta}{2} \cdot \sin \frac{3\theta}{2} \right) \right] \quad 2.6$$

$$\tau_{xy} = \sigma \left(\frac{a}{2r} \right)^{1/2} \left[\sin \frac{\theta}{2} \cdot \cos \frac{\theta}{2} \cdot \cos \frac{3\theta}{2} \right] \quad 2.7$$

where,

σ = gross nominal stress = P/Wt and $a > r > \rho$.

σ_x = is the stress perpendicular to the crack tip
and in the plane of the crack.

σ_y = is the stress perpendicular to the crack plane,

r is the distance from the crack tip to point P.

θ = is the angle between the crack plane and a line
from point P to the crack tip.

For an orientation directly ahead of the crack ($\theta = 0$),

$$\sigma_x = \sigma_y = \sigma \left(\frac{a}{2r} \right)^{1/2}; \tau_{xy} = 0$$

According to Irwin, these equations indicate that the local stress near the crack depend on the product of the nominal stress, σ and square root of half flaw length, a . He called the relationship, the stress intensity factor, K , where for a sharp elastic crack, in an infinitely wide plate,

$$K = \sigma \sqrt{\pi a} \quad 2.8$$

$$\text{So, } \sigma_x = \frac{K}{\sqrt{2\pi r}} \left[\cos \frac{\theta}{2} \left(1 - \sin \frac{\theta}{2} \cdot \sin \frac{3\theta}{2} \right) \right] \quad 2.9$$

$$\sigma_y = \frac{K}{\sqrt{2\pi r}} \left[\cos \frac{\theta}{2} \left(1 + \sin \frac{\theta}{2} \cdot \sin \frac{3\theta}{2} \right) \right] \quad 2.10$$

$$\tau_{xy} = \frac{K}{\sqrt{2\pi r}} \left[\sin \frac{\theta}{2} \cdot \cos \frac{\theta}{2} \cdot \cos \frac{3\theta}{2} \right] \quad 2.11$$

For general case,

$$K = \alpha \sigma \sqrt{\pi a} \quad 2.12$$

2.9 Application of Fracture Mechanics

The main advantage of the fracture mechanics approach to materials assessment is that test data obtained on laboratory specimens can be used for the selection of materials for specific design considerations [17]. If the plane-strain fracture toughness, K_{IC} , is known together with the stress applied to a component, it is possible to calculate the flaw size necessary to cause failure or, conversely, knowing the maximum size and orientation of flaw present in a component, the stress for failure. So, fracture mechanics can be utilized in designing and predicting service life of pressure vessels and other engineering structures in which subcritical flaw growth or time-dependent fractures such as those stemming from stress-corrosion cracking or fatigue are important [20].

The application of fracture mechanics still is largely restricted to conditions in which general yielding is absent, and thus it cannot be used to analyse mechanical fracturing of tough, low-strength alloys, which yield throughout the component or specimen, long before fracture is initiated.

2.9.1 Fatigue life

The fatigue life of a structure can be thought of as comprising three distinct stages (Fig. 2.12) namely [17]

- (a) Crack initiation,
- (b) Crack propagation and
- (c) Final, fast fracture

The presence of a pre-existing flaw (crack) will act as a stress raiser and in turn, reduce or eliminate the initiation stage. For many design considerations, it is the second stage, that of fatigue crack growth, which is of utmost importance, since it is realistic to assume that some form of discontinuity is initially present in the structure.

As a fatigue crack grows under a constant cyclic load, the stress intensity at the crack tip increases due to the increase in the applied stress and crack length. Eventually the crack grows to a sufficient length that the stress intensity is equal to the critical value, K_{IC} , at which point fast fracture occurs.

2.9.2 Fatigue-crack-growth-rate

The dependence of fatigue crack growth rate upon stress intensity has been verified by many investigations [2]. 'Paris' has proposed a generalised fatigue-crack-growth-rate exponential-power law, namely, that

$$da/dN = C(\Delta K)^n \quad 2.13$$

$$\Delta K = K_{\max} - K_{\min} \quad 2.14$$

where,

a = the crack length,

N = the no of fatigue cycles,

da/dN = the fatigue-crack-growth-rate, and

Δk = range of the stress intensity factor
during one loading cycle.

C and n are constants known as Paris constants ($2 \leq n \leq 5$).

Taking log of the Paris equation,

$$\log \frac{da}{dN} = \log C + n \log \Delta K \quad 2.15$$

If we now plot $\log \frac{da}{dN}$ Vs. $\log \Delta K$, we should get a straight line with $\log C$ as the intercept on the y-axis and n as the slope of the line. However experimental crack growth rate data when plotted in terms of $\log(da/dN)$ versus $\log(\Delta K)$ shows a sigmoidal curve (Fig. 2.13) with varying slopes instead of a single straight line [2]. Here three regimes of growth may be defined.

- (a) the mid-growth-rate region (Regime B in Fig. 2.13) typically da/dN between 10^{-6} and 10^{-3} mm/cycle, where propagation rates are related to ΔK through the Paris relationship, $da/dN = C \Delta K^n$
- (b) the high-growth-rate region (Regime C in Fig. 2.13) where K_{max} approaches K_{Ic} ; and
- (c) the near-threshold region (Regime A in Fig 2.13), where ΔK approaches the crack-propagation threshold ΔK_0 . This is the critical value of stress intensity below which the microcrack becomes a non-propagating crack.

2.9.2.1 Factors affecting crack-growth-rate

Fatigue failure occurs when the crack length reaches a critical length, so it is important to note the factors affecting the crack-growth-rate $\left(\frac{da}{dN}\right)$

Crack-growth-rate, $\frac{da}{dN}$ is a function of

- (i). ΔK , stress intensity factor range during one cycle,
- (ii). Material properties (C, n & E; where C & n are Paris constants and E is young's modulus).
- (iii) Environment (Corrosive Resistance, temperature & frequency) and,
- (iv) Overloading

By Paris equation, $\frac{da}{dN} = C(\Delta K)^n$

which clearly shows that

(a) $\frac{da}{dN} \propto C$ (material parameter) and also $\frac{da}{dN} = f(n)$

(b) $\frac{da}{dN} \propto \Delta K$

where $\Delta K = \Delta\sigma \cdot \sqrt{\pi a} \cdot \alpha$

$\Rightarrow \Delta K \propto \Delta\sigma$

$\propto a$

Moreover $a = f(\text{time})$

So, $\Delta K \propto \Delta\sigma, a, \text{time}$

$\Rightarrow \frac{da}{dN} \propto \Delta\sigma, a, \text{time}$

So, if $\Delta\sigma$ is more, i.e., under overstressing, crack-growth-rate will increase. Similarly with the increase in crack length, crack-growth-rate increases and also as time passes, crack-growth-rate increases

$$(c) \frac{da}{dN} \propto \frac{\Delta K}{E} \Rightarrow \frac{da}{dN} \propto \frac{1}{E}$$

i.e, with the increase in Young's Modulus, crack-growth-rate decreases.

$$(d) \frac{da}{dN} \propto R_c, \frac{1}{f}, T$$

where R_c is corrosive resistance

f is frequency

T is time

So, crack-growth-rate increases with increase in corrosive resistance, decreases with increase in frequency and increases with increase in time.

2.9.2.2 Correlation between Fatigue-Crack-Growth-Rate and Microstructural Variables in Rail steel

Effect of Microstructure

Fowler and Tetelman [26] have demonstrated that the prior austenite grain boundary ferrite retards the fatigue crack propagation in region B. They explained that the partial blunting and crack deflection caused when the crack tip encounter the ferrite layers, may be the possible reason for the retardation of the crack growth.

Using electron fractography of fractured surfaces, it has been established that both the prior austenite grain size [27] and pearlite interlamellar spacing [28] influence the fatigue crack propagation rate. Increasing interlamellar spacing and the prior austenite grain size both reduce fatigue crack propagation rate. However, the influence of prior austenite grain size is more pronounced. It has been shown [29] that decreasing the interlamellar spacing linearly increases the fatigue crack initiation and fatigue endurance limit. The

influence of prior austenite grain size and pearlite colony size on fatigue crack initiation was not significant.

Marich [30] has critically examined the fatigue crack propagation behaviour of different rail steels. He observed that materials with higher critical stress intensity factors (K_{IC}) exhibit lower FCGR as shown in Fig. 2.14.

The effect of specimen orientation on FCGR is not studied and reported. Therefore systematic studies regarding the effect of specimen orientation on FCGR is necessary.

Effect of Inclusion

Shik and Araki [31] have shown that fatigue crack growth rate in high strength carbon steels depends upon the total inclusion content but probably is independent of the inclusion type. But some investigators have contradicted this.

2.10 Testing Standards [32]

American Society of Testing and Materials (ASTM) have specified some standards for different testing. Some of the testing methods used is given below

2.10.1 ASTM E 8-86.

Scope: These methods cover the tension testing of metallic materials in any form at room temperature specifically, the methods of determination of yield strength, yield point, tensile strength, elongation, and reduction of area.

Significance & use :

- (1) Tension tests provide information on the strength and ductility of materials under uniaxial tensile stresses. This information may be useful in comparisons of materials, alloy development, quality control and design under certain circumstances.
- (2) The results of tension tests of specimens machined to standardized dimensions from selected portions of a part or material may not totally represent the strength and ductility properties of the entire end product or its in-service behaviour in different environments.
- (3) These methods are considered satisfactory for acceptance testing of commercial shipments. The methods have been used extensively in the trade for this purpose.

2.10.2 ASTM E 23-86.

Scope: These methods describe notched-bar impact testing of metallic materials by the Charpy (simple-beam) apparatus and the Izod (cantilever-beam) apparatus. These methods will in most cases also apply to tests on unnotched specimens.

Significance & Use:

These methods of impact testing relate specifically to the behaviour of metal when subjected to a single application of a load resulting in multiaxial stresses associated with a notch, coupled with high rates of loading and in some

cases with high or low temperatures. For some materials and temperatures, impact tests on notched specimens have been found to predict the likelihood of brittle fracture better than tension tests or other tests used in material specifications.

2.10.3 ASTM E 647-86a

Scope:

- i. This test method covers the determination of steady-state fatigue crack growth rates from near threshold to K_{max} controlled instability using either compact type , C(T) or center-cracked-tension, M(T) specimens. Results are expressed in terms of the crack-tip stress-intensity factor range (ΔK), defined by the theory of linear elasticity
- ii. Several different test procedures are provided, the optimum test procedure being primarily dependent on the magnitude of the fatigue crack growth rate to be measured.
- iii. Materials that can be tested by this test method are not limited by thicknesses or by strength so long as specimens are of sufficient thickness to preclude buckling and of sufficient planer size to remain predominantly elastic during testing.
- iv. A range of specimen sizes with proportional planer dimensions is provided, but size is variable to be adjusted for yield strength and applied load. Specimen thickness may be varied independent of planer size.

Significance and Use:

- i. Fatigue crack growth rate expressed as a function of crack-tip stress-intensity factor range, da/dN versus ΔK , characterises a materials resistance to stable crack extension under cyclic loading. Expressing da/dN as a function of ΔK provides results that are independent of planer geometry, thus enabling exchange and comparisons of data obtained from a variety of specimen configurations and loading conditions.
- ii. This test method can serve the following purposes .
 - (a) To establish the influence of fatigue crack growth on the life of components subjected to cyclic loading, provided data are generated under representative conditions and combined with appropriate fracture toughness data.
 - (b) To establish material selection criteria and inspection requirements for damage tolerant applications.
 - (c) To establish, in quantitative terms, the individual and combined effects of metallurgical, fabrication, environmental, and loading variables on fatigue crack growth.

2.11 Mechanical Properties Assessment

Conventionally we measure tensile, notched tensile, charpy C_{VN} , hardness mainly. But in presence of cracks in the structures under fatigue loading conditions, we have to opt some other safety assessment parameter of the structural material properties which can be found out by using F.M. techniques, for example, by finding out Fracture toughness, crack tips and also correlating these F.M. parameters which can lead us to the assessment of the safety of structural components.

EXPERIMENTAL PROCEDURE

3.1 Materials

The materials investigated were given by RDSO to the Welding Research Laboratory, Roorkee. These were head hardened high strength rails and medium manganese rails.

3.2 Microstructural studies

Specimens of 40 mm length and $10 \times 10 \text{ mm}^2$ cross section were prepared from head hardened rails for the microstructural studies, one in each longitudinal, transverse and short-transverse directions respectively after polishing mechanically following the standard metallographic procedure. Microstructure was seen on optical microscope (Make-Leitz.) and micrographs were taken at a distance of 6 - 8 mm along the specimen. Etchant used was 5% nital solution (5 ml nitric acid and 95 ml methanol). The locations of the specimens in the rail section is shown in Fig. 3.1.

3.3 Hardness Tests

After taking the microstructure, hardness were taken at a distance of 5 to 6 mm along the length of the specimen. Microhardness was taken on micro-hardness

testing machine (Make-Leitz.) with a weight of 10 mg and macrohardness was taken on hardness testing machine (Make-Wolpert.) with a weight of 5 kg. The hardness scale selected was Vickers. The diagonals of the indentation were measured and after taking the average, the hardness values were read from the standard table corresponding to the weight applied.

3.4 Tensile Tests

Tensile specimens three in each direction of standard dimensions (Fig. 3.2) corresponding to ASTM E 8-86 [32] were made from medium manganese rails. The longitudinal and transverse specimens were machined from the head and short-transverse specimens were machined from the head and the web. The location of the test specimens in the rail section is shown in Fig. 3.3.

The 0.2% offset yield strength, ultimate tensile strength, % elongation at fracture and % reduction of area were determined using servo-hydraulic universal testing machine (Make-MTS).

3.5 Impact Tests

Impact specimens (Charpy V-notch type) of standard dimension (Fig. 3.4) corresponding to ASTM E 23-86 [32] were made from head hardened rails in the three directions. 8-10 specimens were machined from the head of the rail in the longitudinal, transverse and short-transverse directions and were tested at 3 temperatures (0°C; Room temperature = 25°C; & 70°C) on pendulum type impact machine (Make-FTM).

The locations of the test specimens is shown in Fig. 3.5. The energy required to break the specimen upon applying impact load was measured by the pointer position on the dial and was recorded in terms of Joule.

3.6 Fatigue-Crack-Growth-Rate (FCGR) Tests

Compact type, C(T) specimens were made as per ASTM E 647-86a [32]. The dimensions of the specimens were $W = 60$ mm and $B = 15$ mm ($W =$ Width; $B =$ Thickness). The specimen drawing is given in Fig. 3.6. For the determination of FCGR, the specimens were at first fatigue pre-cracked upto $a/W = 0.26$ to 0.3 depending on the initial notch depth of the specimen. The specimens were fatigue pre-cracked in a 600 KN servo hydraulic universal testing machine (Make-MTS). The whole pre-cracking of the specimens were done with decreasing load. The final K_{max} during pre-cracking was kept below the initial K_{max} for which test data are to be obtained.

To pre-crack the specimens, the loads corresponding to K_{max} equal to 30-35 $MPa\sqrt{m}$ were used to cause initial pre-cracking at the machined notch. Later on, the load was stepped down to achieve the requirement of a K_{max} value of 20 $MPa\sqrt{m}$. The total pre-crack length, a_0 , was given as 3.75 mm ($a_0 = W/16$ or $0.1 B$ or 1 mm; whichever is greater). For conducting the FCGR test, the specimen was again pre-cracked for further 0.5 mm at $K_{max} = 19.5 MPa\sqrt{m}$.

Then finally, FCGR test was done at frequency, $f = 15$ Hz, stress ratio, $R = 0.1$, and $K_{max} = 20 MPa\sqrt{m}$ under load control mode. The final crack length given was 30-32 mm.

The location of the specimen in the rail section is shown in Fig. 3.7. A single specimen was made in each direction. These specimens were taken from

head-hardened rails because the smallest grip available in the lab was for 15 mm thickness specimen and these could not be machined from the medium-manganese rails. The specimens had notch direction in longitudinal, transverse and short-transverse respectively. For the specimen having notch in the short-transverse direction, the notch was made in the lower portion, so that the crack growth takes place completely in the head portion. Due to shortage of time, only two specimens having notch in longitudinal and short-transverse direction were tested.

RESULTS AND DISCUSSIONS

4.1 Results

4.1.1 Chemical composition

The chemical composition of the medium manganese and the head hardened rails is given in Table 4.1. The chemical composition was found to be same in the three direction.

4.1.2 Microstructure

The specimens etched in 5% Nital Solution were observed under optical microscope (Make-Leitz). There was no change in microstructure in the longitudinal and the transverse directions, but there was change in the microstructure along the short-transverse directions. The grains coarsened on moving towards the web portion. The microstructures are shown in Fig. 4.1.

4.1.3 Hardness Tests

The hardness tests, revealed that the hardness values were constant in the longitudinal direction and varied in the transverse and the short-transverse direction. The macro and the micro-hardness tests values are given in Tables 4.2

and 4.3 respectively. On moving from the centre to the side of the transverse specimen the macro hardness decreased. In the short-transverse specimen, the macro-hardness decreased on moving from top to bottom (i.e., from the head to the web). Same pattern was observed in then micro-hardness measured. But the micro-hardness values of black and white portions were different. White portion had higher micro-hardness values than the black portion.

4.1.4 Tensile Tests

The tensile test results are given in Table 4.4 and Figs. 4.2 to 4.9. From the results, one can see that the yield strength and the ultimate strength is highest in the transverse direction and lowest in the Short-transverse-direction. Reduction of area, (R.O.A) is highest in the longitudinal direction and lowest in the transverse direction and intermediate in the short-transverse direction. Elongation at fracture, (E.A.F) is highest in the longitudinal direction and lowest in the short-transverse direction, and intermediate in the transverse direction.

4.1.5 Impact Tests

The impact test results are given in Table 4.5. It is known that the impact tests give very much scattered results, but still the transverse specimens gave the lowest value at each temperature. Also as the temperature increases, the impact values in different direction increases.

4.1.6 Fatigue-Crack-Growth-Rate (FCGR) Tests

The FCGR test results are given in Tables 4.6 and 4.7 and Figs 4.10 and 4.11. Fig. 4.10 and Table 4.6 correspond to transverse specimen with notch in the longitudinal direction, here after referred as specimen-1. Fig 4.11 and Table 4.7 correspond to longitudinal specimen with notch in the short-transverse direction, here after referred as specimen-2.

4.2 Discussion

4.2.1 Microstructure

Generally the cooling rate in the web is higher than the head as the head is thicker in section than the web and acts as a large reservoir of heat. So the web portion must have fine grain size and the head portion must have coarse grain size. But in the head hardened rails, the head is heated by an induction coil shaped in the form of inverted U. After this they are quenched in steam and air. This quenching gives finer grain size and the residual heat which escapes in the web coarsens its structure. Therefore coarse grain size has been obtained in the web and fine grain size in the head.

4.2.2 Hardness

The hardness values are found to be lower in the web and higher in the head which may be due to coarsening of the grains in the web. Also due to compression of the head from both the sides, the metal in the centre portion of the head (when considering transverse direction) undergoes maximum deformation and so its

hardness is higher as compared to the sides. The hardness values are found to be same along its length in head portion which may be attributed to the same microstructure and deformation

4.2.3 Tensile Tests

The yield strength and the ultimate strength is highest in the transverse direction because the grains are compressed in this direction and the specimen made is perpendicular to the grain alignment. So the load is applied perpendicular to the grain alignment. The yield strength and the ultimate tensile strength must be lowest in the longitudinal direction as the grains and inclusions are already elongated in this direction, but the yield strength and the ultimate strength is lowest in the short-transverse direction, because the specimen extracted in the short-transverse direction is from the head and the web portion. The web portion has coarser grain size and it is comparatively less harder than the head, so this reduces the overall strength in the short-transverse direction. Reduction of Area(R.O.A.) & elongation at fracture (E.A.F.) is highest in the longitudinal direction because the specimens are oriented parallel to the grain alignment direction. R.O.A. is lowest in the transverse direction because the load is applied across the grain and the inclusion alignment, therefore conforming to maximum ultimate strength in the transverse direction.

4.2.4 Impact Tests

The transverse specimen gives the lowest value at each temperature, because the V-notch is made in the longitudinal direction along which the inclusions are

found to be aligned (as seen in the microstructure). As the temperature increases, the impact values increases in different directions because, at low temperature the material fracture changes from ductile to brittle. Higher the brittleness, lower will be the impact values.

4.2.5 Fatigue-Crack-Growth-Rate Tests

In specimen-1, in which notch is in the longitudinal direction, the crack will grow along the grain alignment and in specimen-2, in which notch is in the short-transverse direction, the crack will grow across the grain alignment. So in specimen-1, the crack finds easy to propagate as compared to crack in specimen-2. It was found by Upendra [15] that the difference arises due to the inclusion orientation effect. The crack plane of the specimens with TL-(T = Transverse; L = Longitudinal) orientation (specimen-1) contained sulfide inclusions with their axes parallel to crack-propagation direction. He said that the nature of inclusion morphology in the crack plane plays an important role in controlling the fatigue crack growth rate.

So, one can see from the Tables 4.6 and 4.7 and figs.4.10 and 4.11 that the initial-crack-growth-rate is lower in specimen-1 and higher in specimen-2, where as the final-crack-growth-rate is higher in specimen-1 and lower in specimen-2. The initial crack-growth-rate depend on the initial notch length and the final crack-growth-rate depends on the total crack length. The increase in crack-growth-rate can be compared in the two specimens by considering the slope of the line i.e., the value of n . n is higher in specimen-1 than in specimen-2, so the increase in crack-growth is higher in specimen-1.

CONCLUSIONS

Following can be concluded from the present investigation on high strength head hardened & medium Mn rails.

- (1) The chemical composition is same in all the three directions, i.e. longitudinal, transverse and short transverse directions in the above rails.
- (2) The grain size is nearly same in the transverse and longitudinal direction in head hardened rails, and the grains get coarsened as one moves from the head to the web. So, there was variation in grain size in the short-transverse direction.
- (3) The microstructural studies of head-hardened rails revealed that the black portion in the head may be fine pearlite and white portion may be acicular ferrite. The black portion in the web may be coarse pearlite and white portion may be ferrite.
- (4) The hardness is same in the longitudinal direction, but it decreases in the short-transverse direction in head hardened rail from the head to the web, and in the transverse direction, it is maximum at the centre and decreases on either side.

- (5) The tensile strength of medium Mn rails is highest in the transverse direction and lowest in the short-transverse direction and intermediate in the longitudinal direction.
- (6) The impact values for head hardened rail is lowest in the transverse direction and highest in the longitudinal direction.
- (7) The crack finds more easy to propagate in the longitudinal direction than the short-transverse direction.

SCOPE FOR FUTURE WORK

As the rails are made with various composition, and with various heat treatment, so more detailed investigation, in all the three directions for similar types of rails shall be furthered so that an accurate assessment of similar type and of dissimilar type of failure can be made more accurately to predict the failure behaviour of various types of rails. Further more, fatigue crack, which in general propagates in the form of striations, in the present case it has been observed that these striations were of larger dimensions which in literature has been termed as pop-in. Further investigation on this aspect can provide some important facets about the catastrophic fatigue fracture of rails, in terms of perhaps its causes, mechanisms and subsequently its prevention and prediction of these types of catastrophic fatigue failures.

REFERENCES

1. Broek, D., "Elementary Engg. Fracture Mechanics", pp. 304-309, 1982.
2. Papers presented at the 1978 ASM Materials Science Seminar, "Fatigue and Microstructure", pp. 83-86, 1979.
3. Hanson, A. and Parr, J.G, "The Engr's Guide to Steel", pp. 201-203, 1965.
4. Sharp, H.J., "Engg. Materials", pp. 302-306, 1966.
5. Pickering, F.B., "Physical metallurgy and the design of steels", pp. 89-100, 1978.
6. Lankford, W.T., Samways, N.L., Craven, R.F. and McGannon, H.E., "the making shaping and treating of steels", 10th ed., pp. 889-900, 1985.
7. Smith, Y.E. and Fletcher, F.B., "Alloy steels for high strength; As rolled rails: Rail steels-Development, processing and use, ASTM, STP-644, pp. 212, 1978.
8. Tamura, Y., Irie, T., Naguchi, T., Ueda, M., Tanaka, M and Ide, T., "Development of the heat treatment of rails", Nippon Kokkan, Technical report No. 29, pp. 10, 1980.
9. Ackert, R.J., Witty, R.W. and Grozier, P.A., "Method for the production of improved railway rails by accelerated cooling in line with the production rolling mill US Pat. No. 4, pp. 248, 486, Dec. 4, 1984.
- 10 Stone, D.H. and Steele, R.K., "The effect of mechanical properties upon the performance of railroad rails", ASTM, STP-644, pp. 21, 1978.
11. A short term course on, "Welding Technology", under Q.I.P., I.I.T., Delhi, pp. 7.1 to 7.16, 1990.

12. Biggs, W.D., "The brittle fracture of steel", McDonald and Evans, 1960.
13. Shank, M.E., "Brittle behaviour of Engg. structures", New York, John Wiley and Sons, 1957.
14. "Fatigue crack propagation", ASTM special technical publication, No. 415, 1967.
15. Singh, U.P., "Fatigue and fracture studies of rail steels", PHd. Thesis, I.I.T., Bombay, 1988.
16. Rosenfield, A.R., "Metall. Rev.", pp. 13, 29, 1968.
17. "Metals Handbook", 9th ed., Vol.8, A.S.M., Metals Park, Ohio, pp. 437-491, 1985.
18. Dieter, G.E., "Mechanical Metallurgy", 3rd ed., pp. 348-374, 1987.
19. Paris, P.C., and Sih, G.C., "Stress Analysis of Crack", ASTM, STP-391, pp.30-81,1965.
20. "Fracture Toughness", The Iron and Steel Institute, London, 1968.
21. Wilshaw, T.R., Rau, C.A. and Tetelman, A.S., "Engg. fracture Mechanics", pp. 1, 191, 1968.
22. Rodrigues, P., "Fracture Toughness Evaluation-A historical perspective", Trans Inidan Inst. Met., Journal, Vol. 46, No. 5, pp. 265-296, Oct. 1993.
23. Shioya, T., "Analysis of crack propagation in brittle Materials", JSME International Journal, Series A, Vol. 37, No. 1, 1994.
24. Parker, A.P., "The mechanics of fracture and fatigue", 1st ed., pp. 21-22, 1981.
25. Irvin, G.R., "Trans. ASM", 40A, pp. 147, 1948.
26. Fowler, G.J., and Tetelman, A.S., "The effect of grain boundary ferrite on fatigue crack propagation in pearlitic rail steels, Rail steels-developments, processing and use", ASTM, STP-644, pp. 363, 1978.

27. Gay, G.T., Thompson A.W., Williams, J.C., and Stone, D.H., "The effect of microstructure on fatigue crack propagation in Pearlitic Eutectoid Steels", Canadian Metallurgical Quarterly, 21 (1), pp. 73, 1982.
28. Sunwoo, H., Fine, M.E., Meshii, M. and Stone, D.H., "Cyclic deformation of Pearlitic Eutectoid Rail Steel", Met. trans., 13A, pp. 2035, 1982.
29. Gray, G.T., Thompson, A.W. and Williams J.C., "Influence of Microstructure on Fatigue crack initiation in fully pearlitic steels", Metl Trans., 16A, pp. 753, 1985.
30. Marich, S., "Vanadium in rail steels (Proc. Seminar)", BIIP Melb. Res. Lab., Chicago, pp. 23, 1973.
31. Shin T. and Araki T., Trans. ISIJ, 13(1), pp. 11, 1973.
32. Annual Book of ASTM standards, "Metals test methods and analytical procedures", 1990.

L=Longitudinal
 T=Transverse
 ST=Short transverse

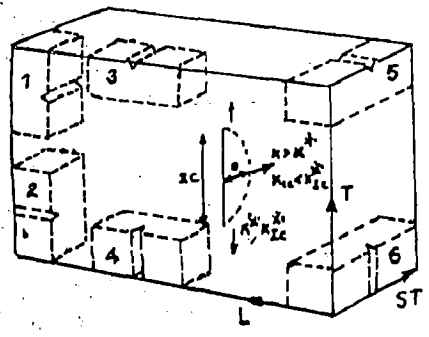


Fig.2.2 : Direction of crack growth in rolled plate.[1]

Spec	Axis	Crack
1	T	L
2	T	ST
3	L	T
4	L	ST
5	ST	T
6	ST	L

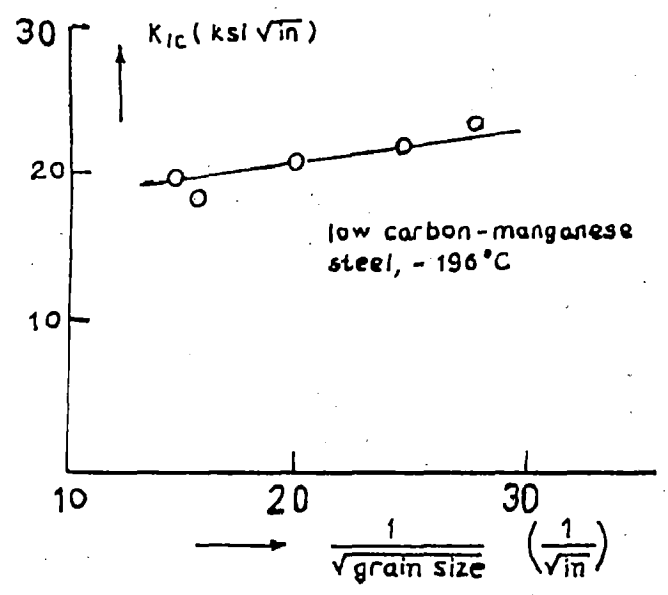


Fig. 2.1: Effect of grain size on toughness [1]

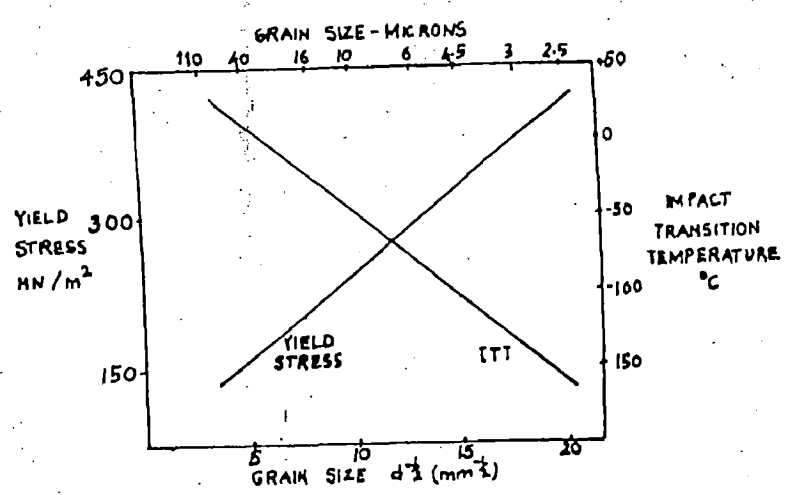
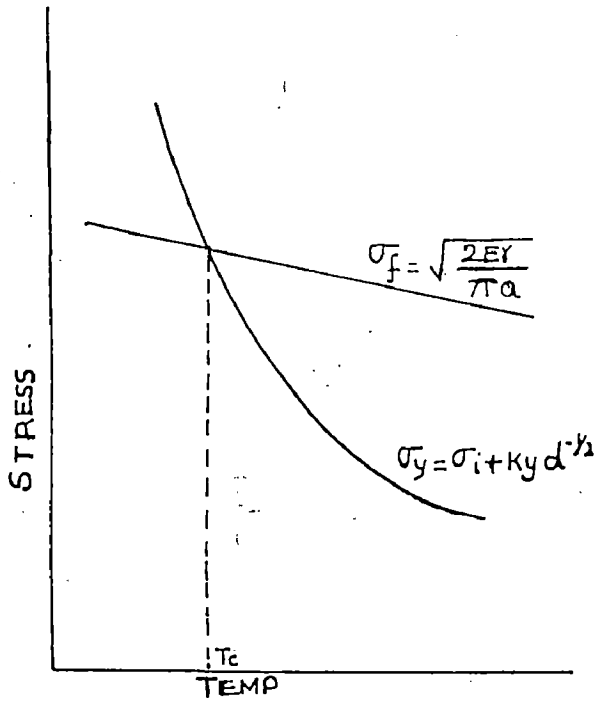
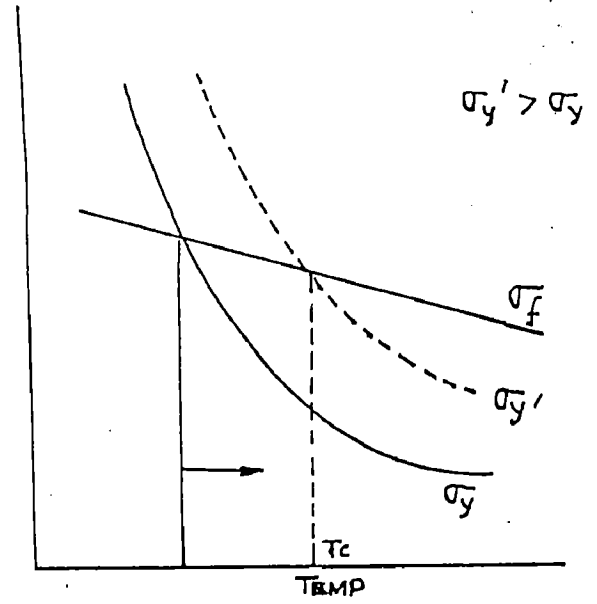


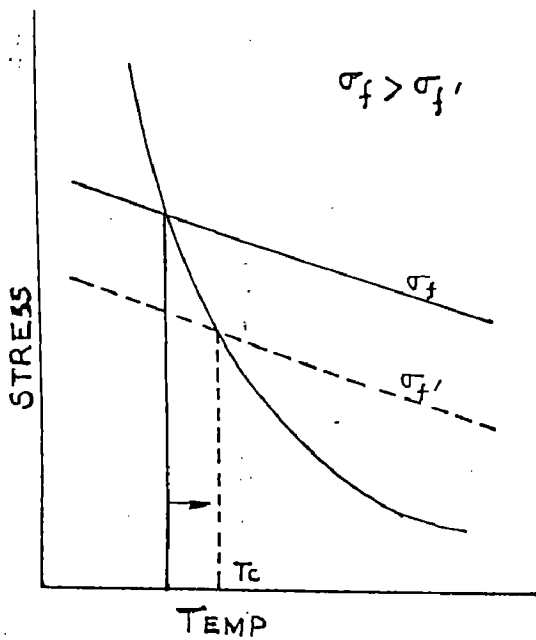
Fig. 2.3 : Effect of ferrite grain size on the impact transition temperature and yield strength of a 0.1% C steel [11]



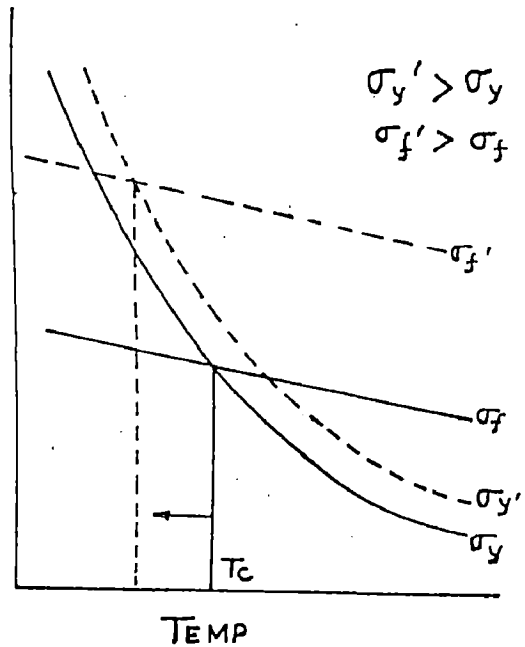
(a) showing derivation of T_c



(b) effect of increasing σ_y



(c) effect of decreasing σ_f



(d) effect of grain refinement

Fig.2.4: Schematic variation of fracture stress (σ_f) and yield stress (σ_y) with temperature for steel. [11]

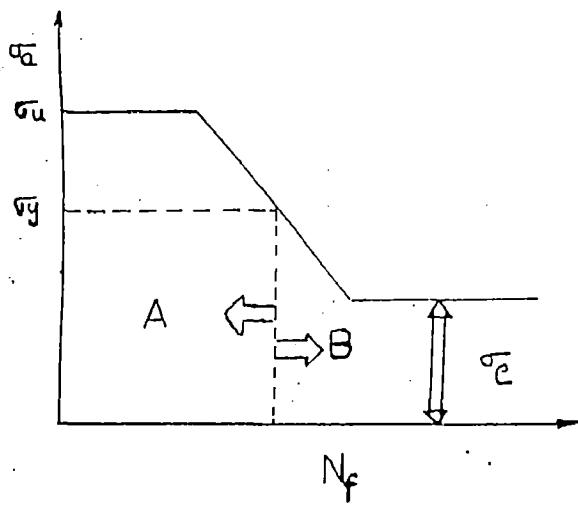


Fig. 2.5 : Plot between number of cycles to failure and stress amplitude

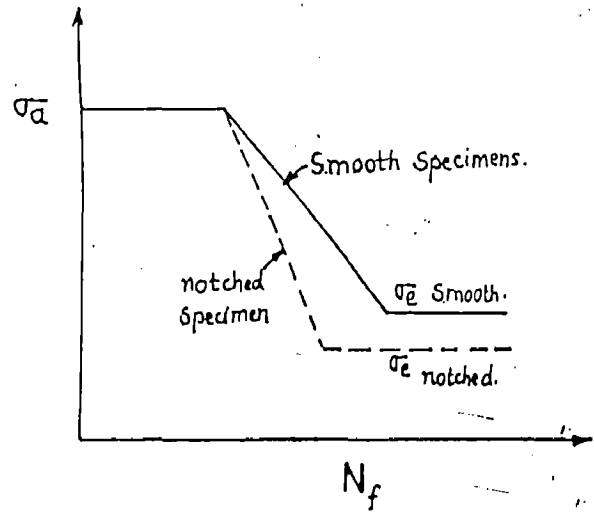


Fig. 2.6 : Plot between N_f Vs σ_a showing effect of notch

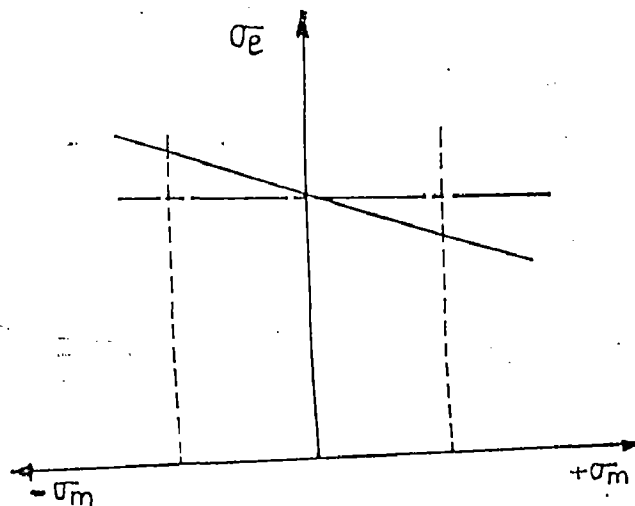


Fig. 2.7 : Plot showing effect of mean stress on σ_e

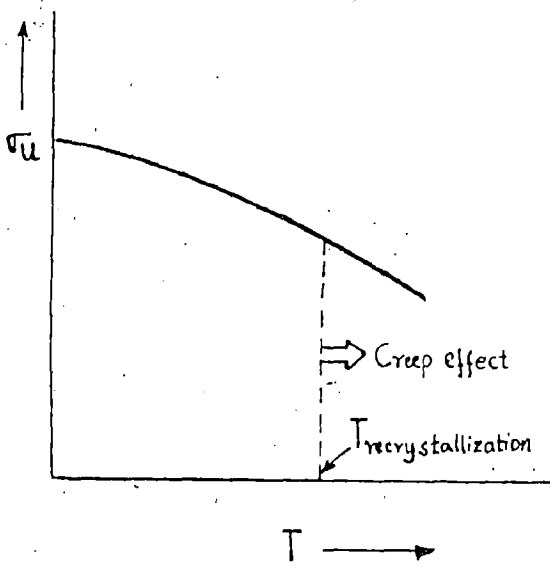


Fig.2.8 : Plot showing effect of temperature on σ_u

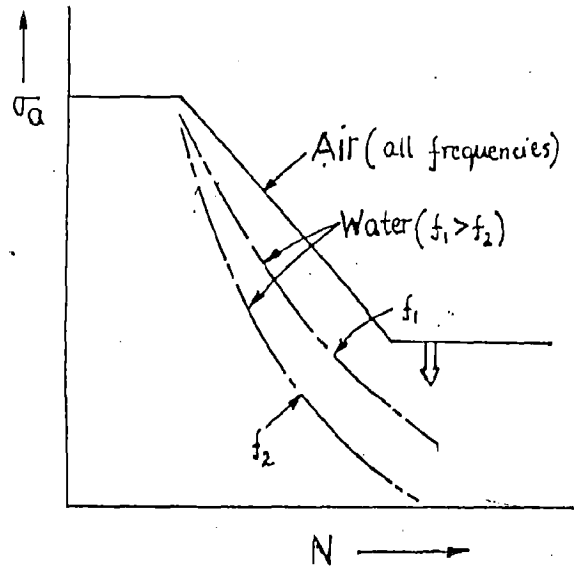


Fig.2.9 : Plot showing effect of corrosive environment on σ_a

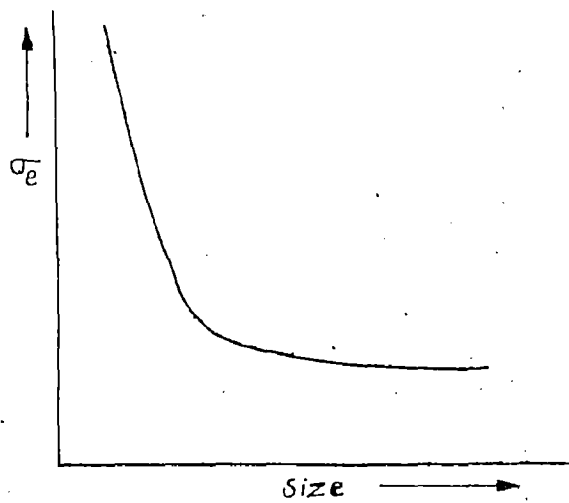


Fig.2.10 : Plot showing effect of size on σ_e

247319



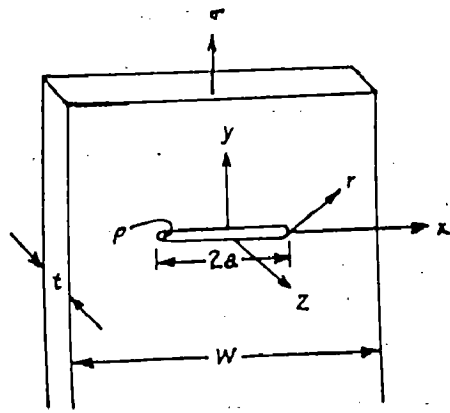


Fig. 2.11 Model for equations for stresses at a point near a crack [18]

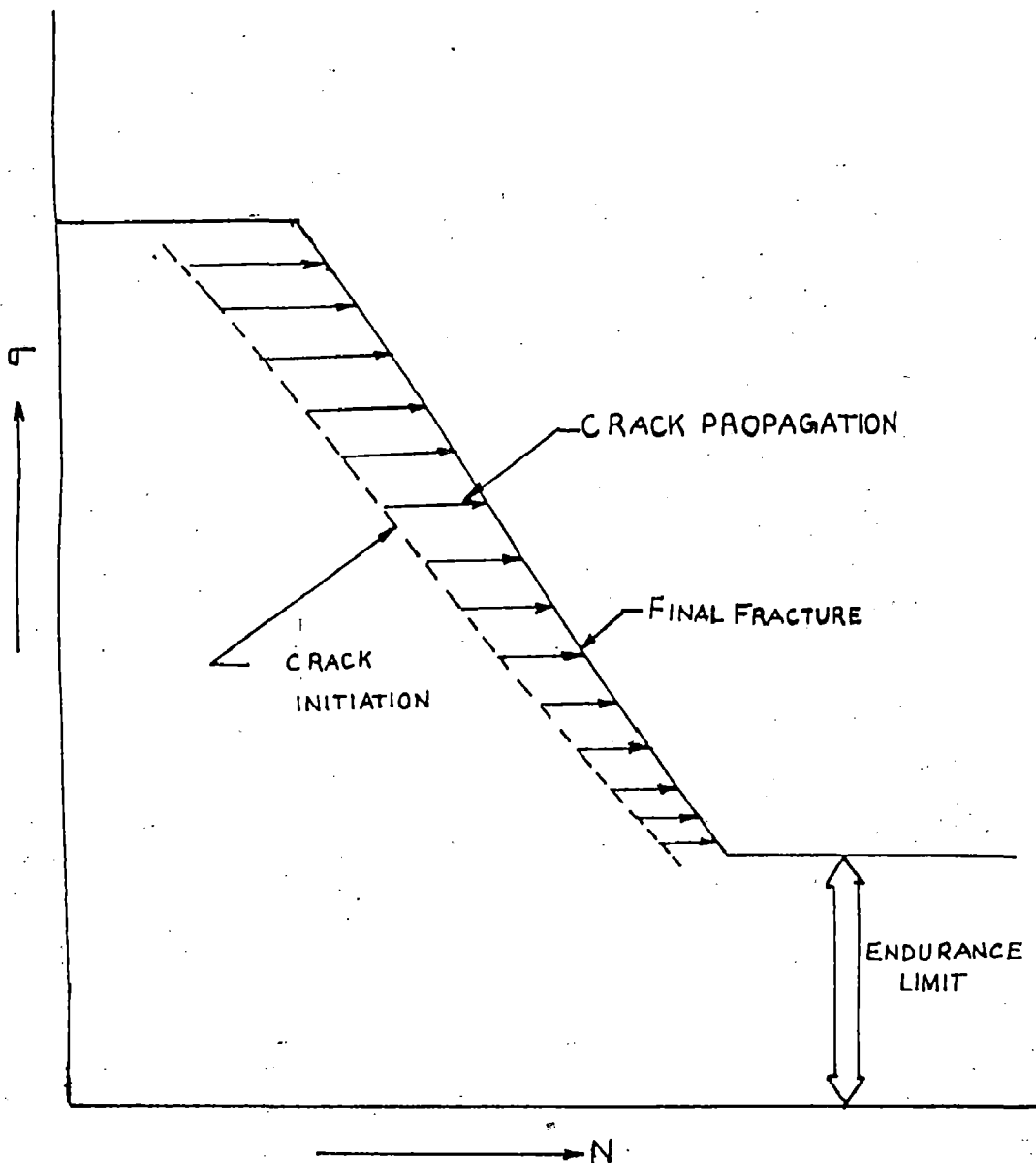


Fig. 2.12 : Effect of fatigue crack growth on S-N curve.

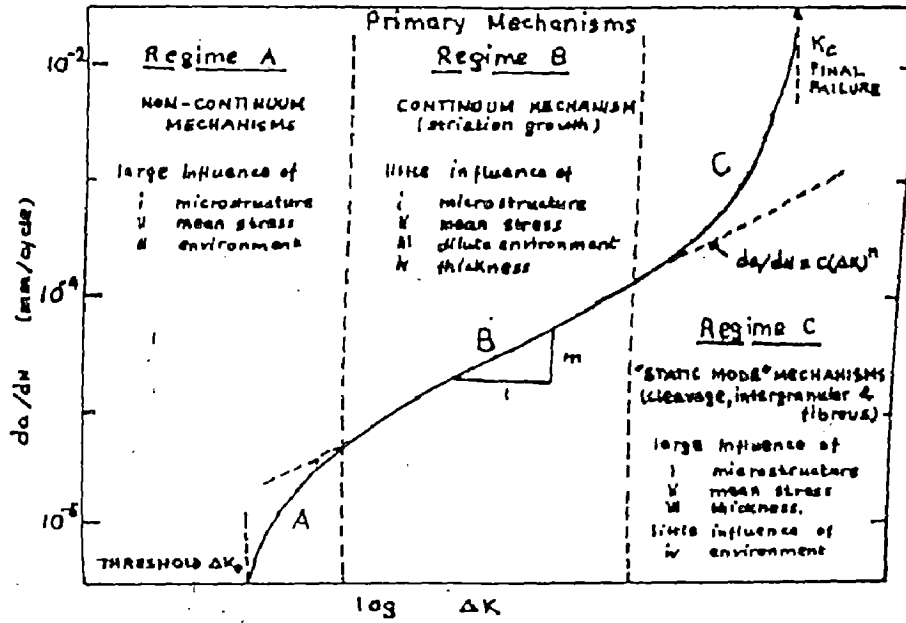


Fig. 2.13 Schematic variation of fatigue-crack growth rates (da/dN) with alternating stress intensity (ΔK) [11]

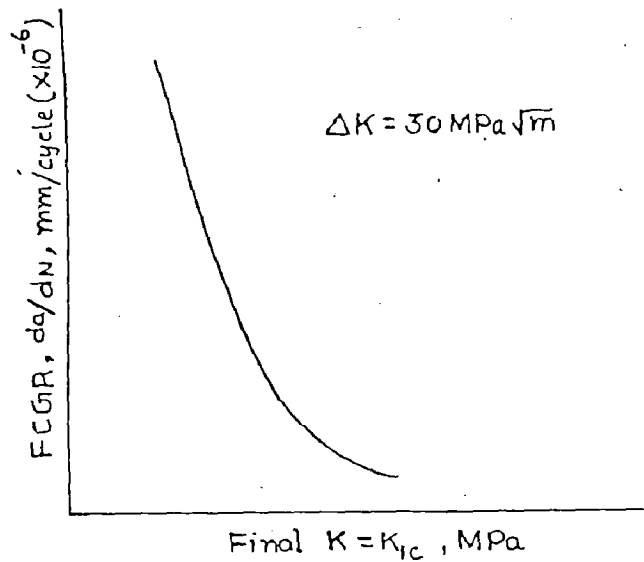


Fig. 2.14 : Variation of fatigue crack growth rate (FCGR) with K_{1C} .

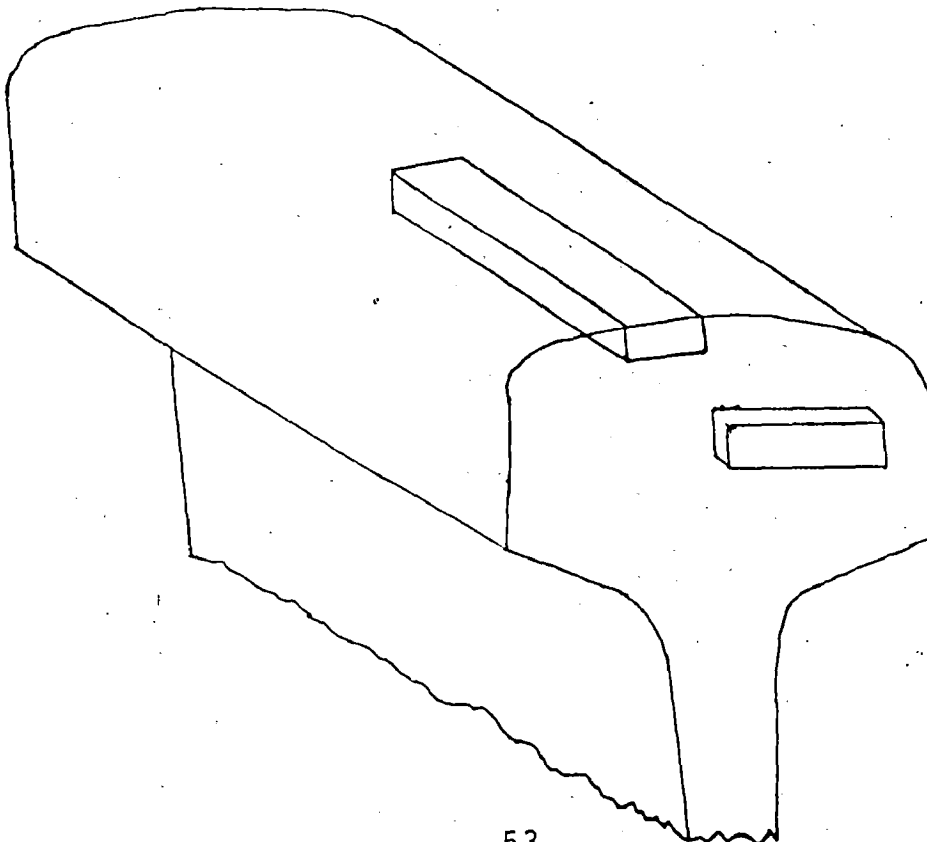
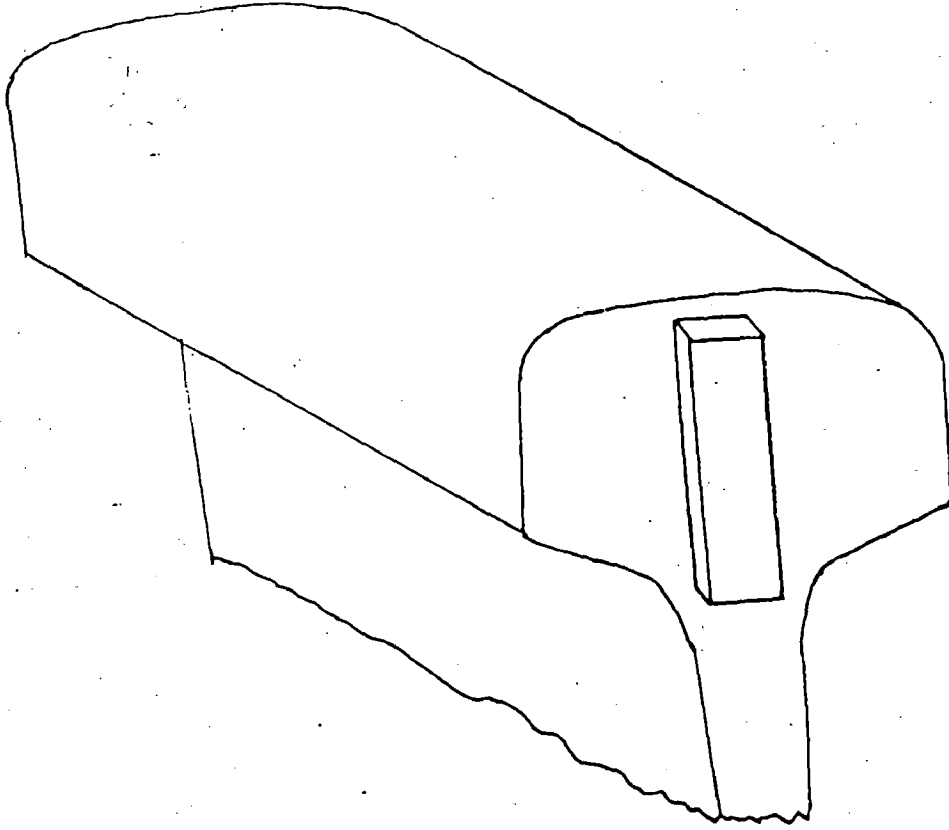


Fig. 3.1 : Location of specimen for hardness and microstructural studies

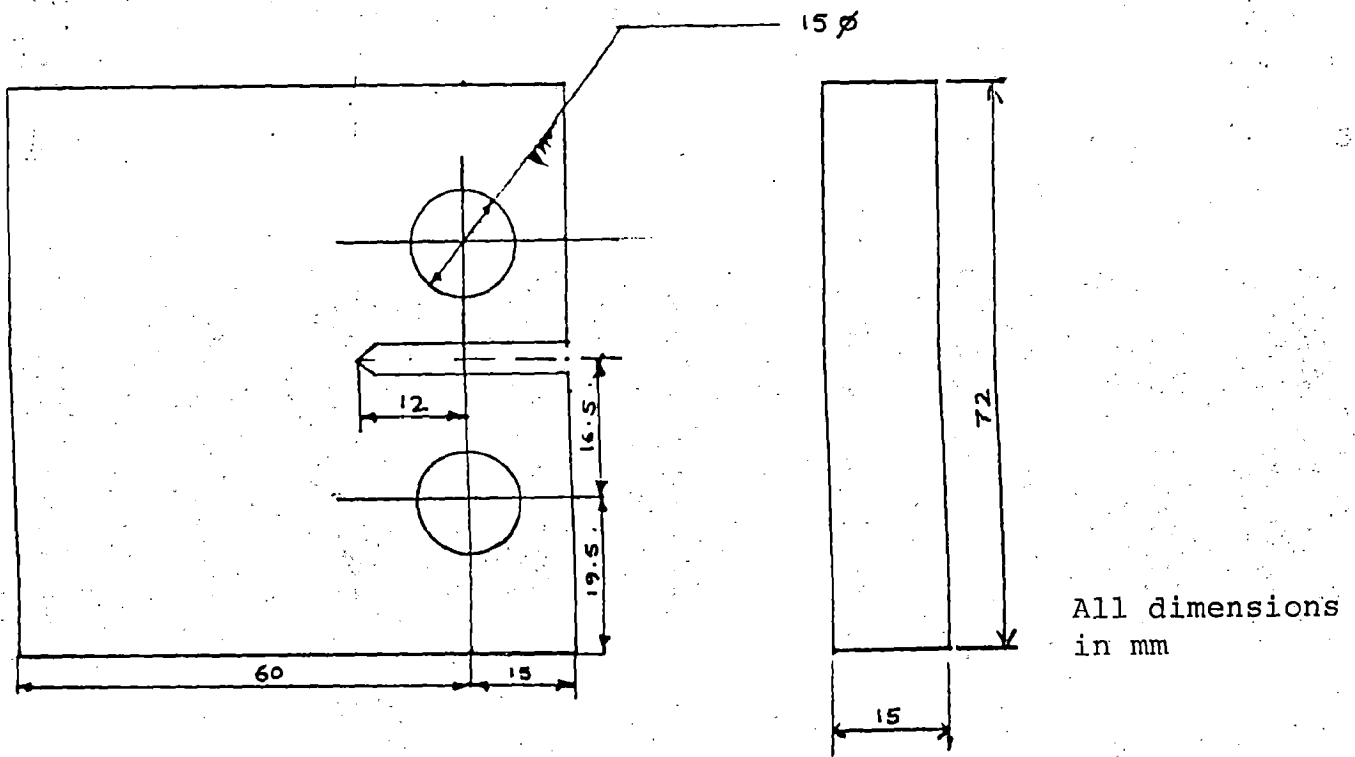


Fig. 3.6 : Drawing of C.T. specimen

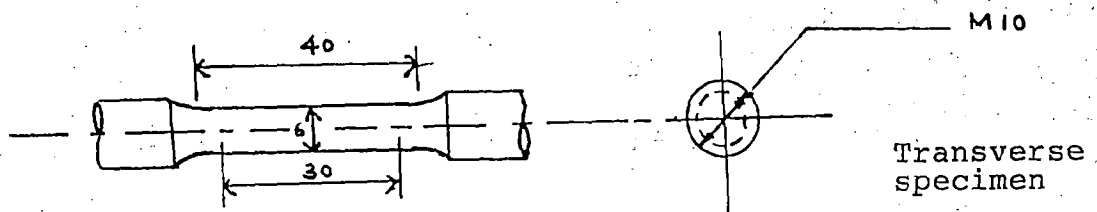
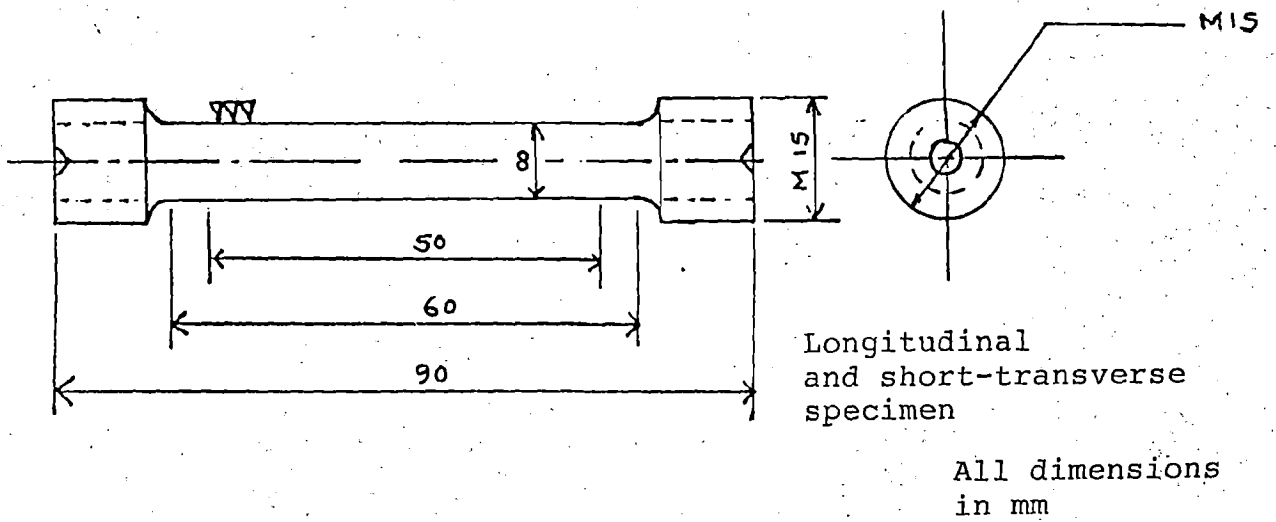


Fig. 3.2 : Drawing of the tensile specimen.

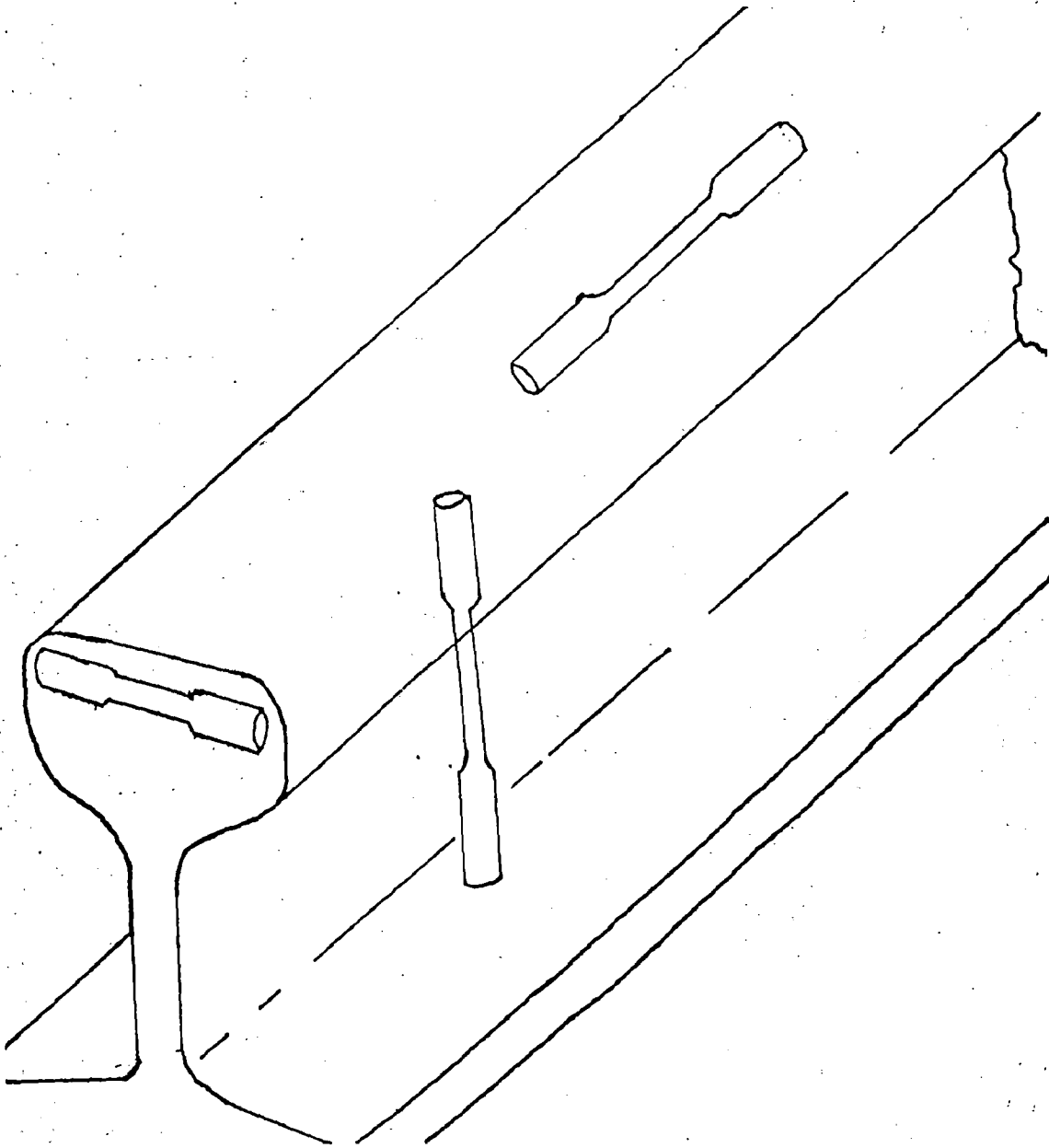
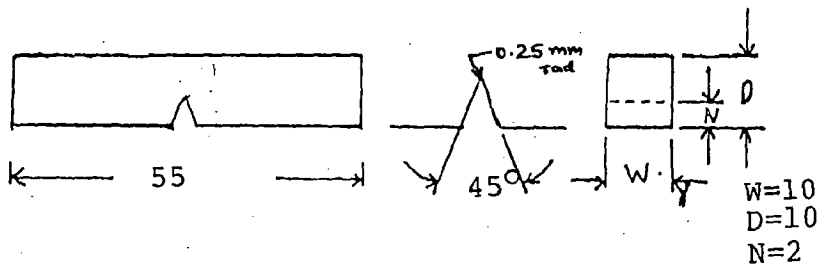
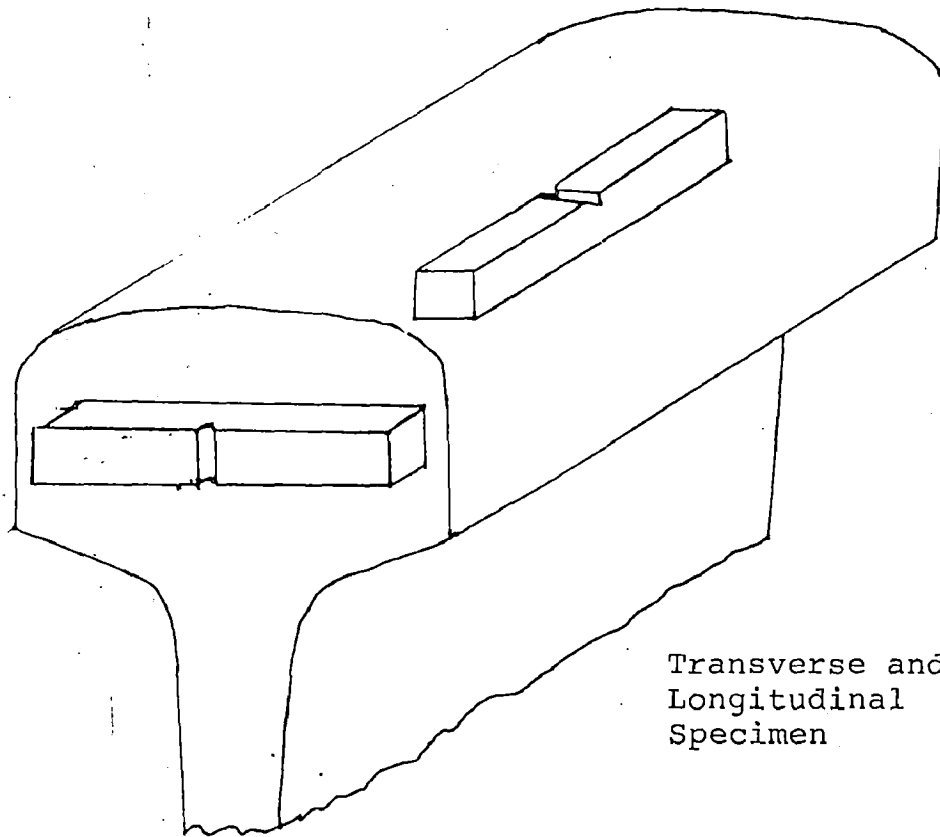


Fig. 3.3 : Location of tensile test specimen in the rail section.

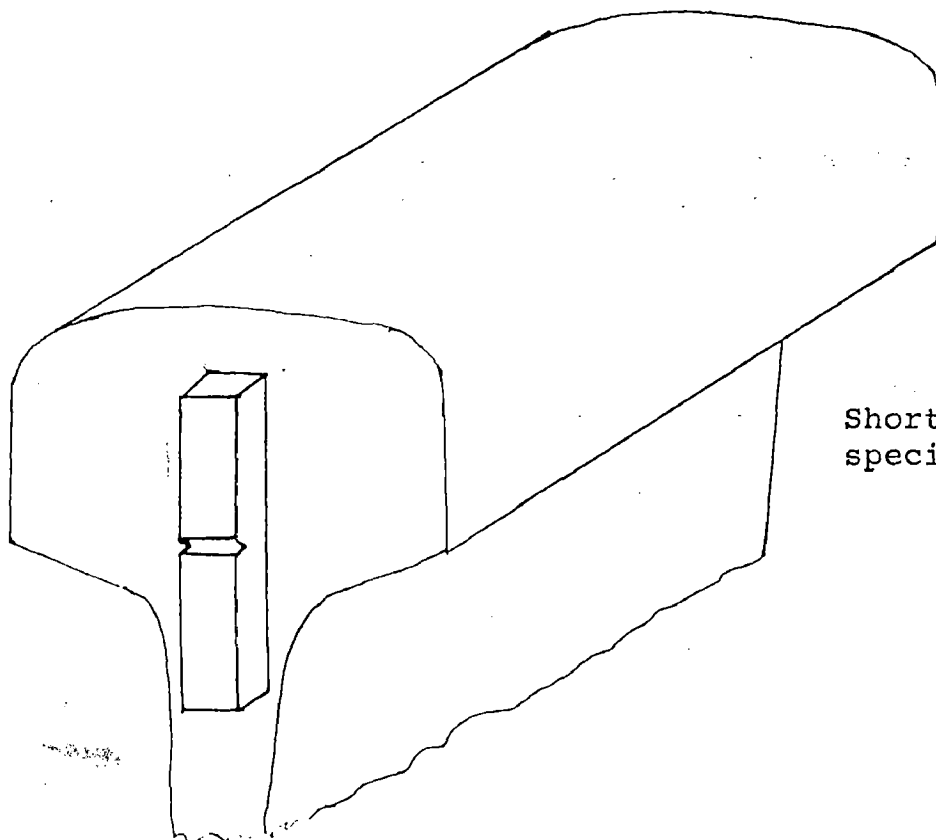


All dimensions in mm

Fig. 3.4 : Drawing of the impact specimen.

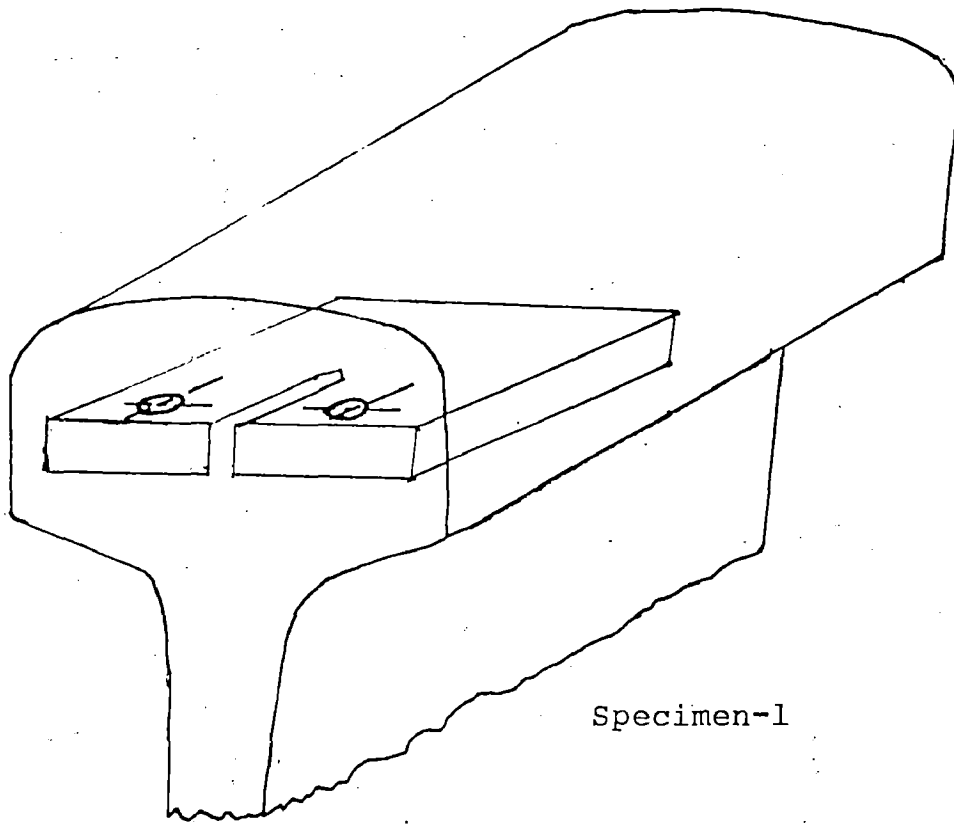


Transverse and
Longitudinal
Specimen

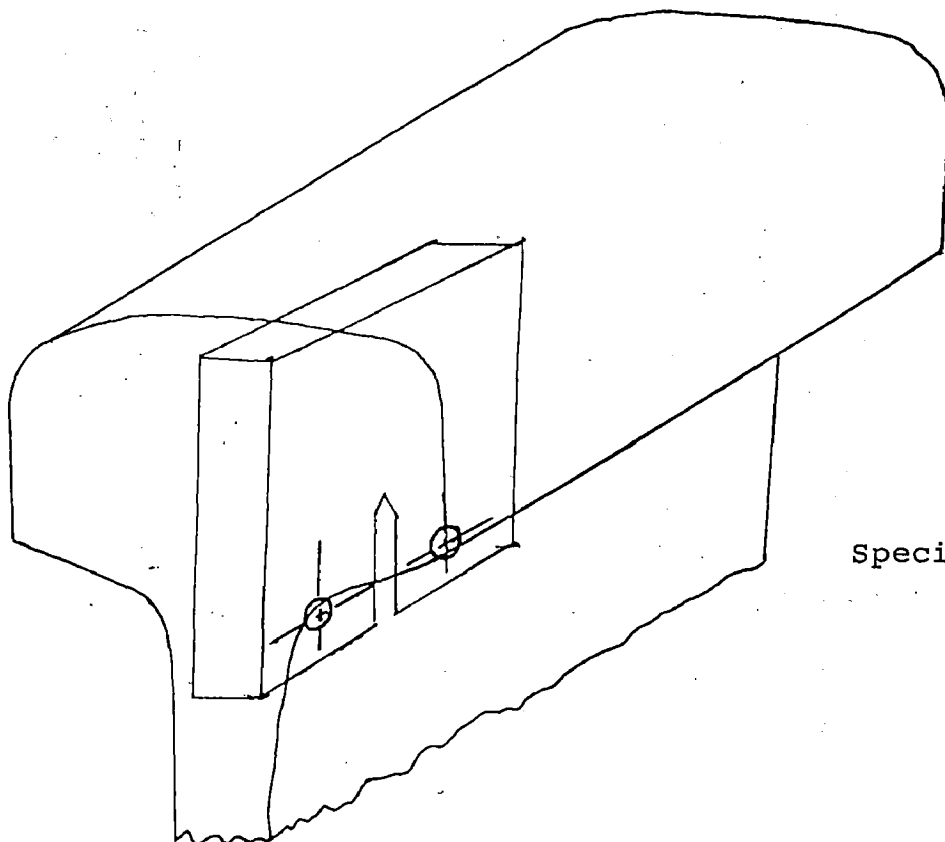


Short-transverse
specimen

Fig. 3.5 : Location of the impact specimen in the rail section.

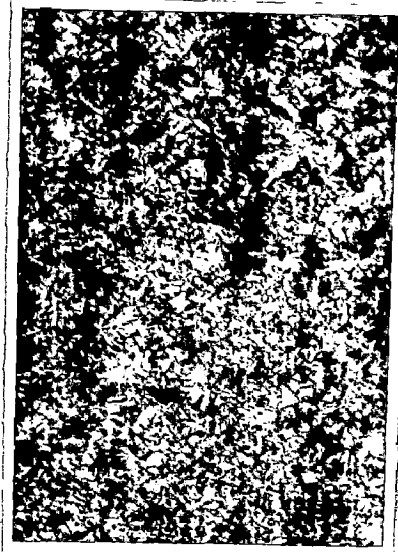


Specimen-1



Specimen-2

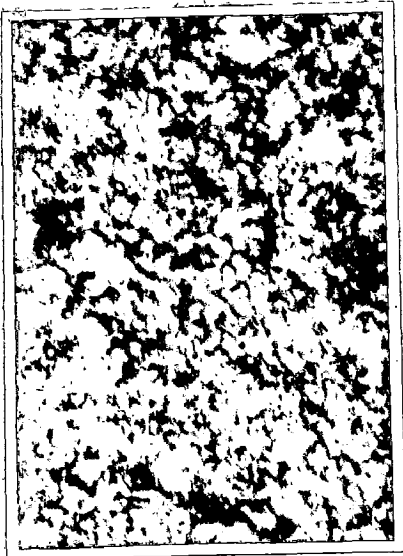
Fig. 3.7 : Location of the C.T. specimen in the rail section



(i)



(ii)



(iii)

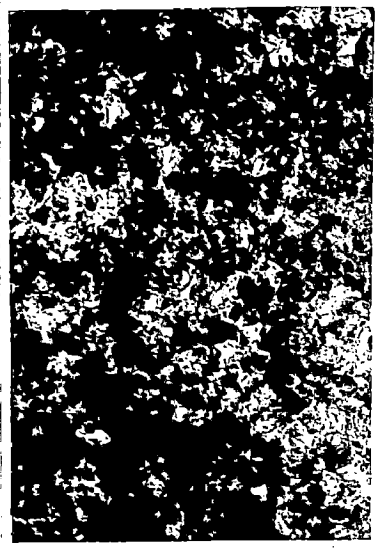
Fig. 4.1a : Micrographs of longitudinal specimen.
(along the length)

Etchant used : 5% Nitral Soln

Magnification : X100



(i)



(ii)



(iii)



(iv)



(v)



(vi)

Fig. 4.1b : Micrographs of transverse specimen.
(Centre to side)

Etchant used : 5% Nital Soln

Magnification : X 250



(iv)



(v)



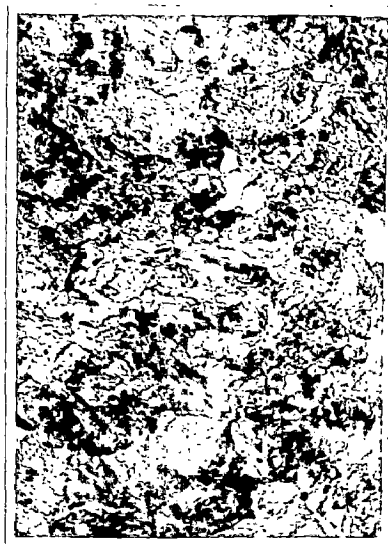
(vi)



(vii)



(viii)



(ix)

Fig. 4.1c : Micrographs of short transverse specimen.
(head to web)

Etchant used : 5% Nitro soln

Magnification : X 250

Sample Id: MDAIAM #1

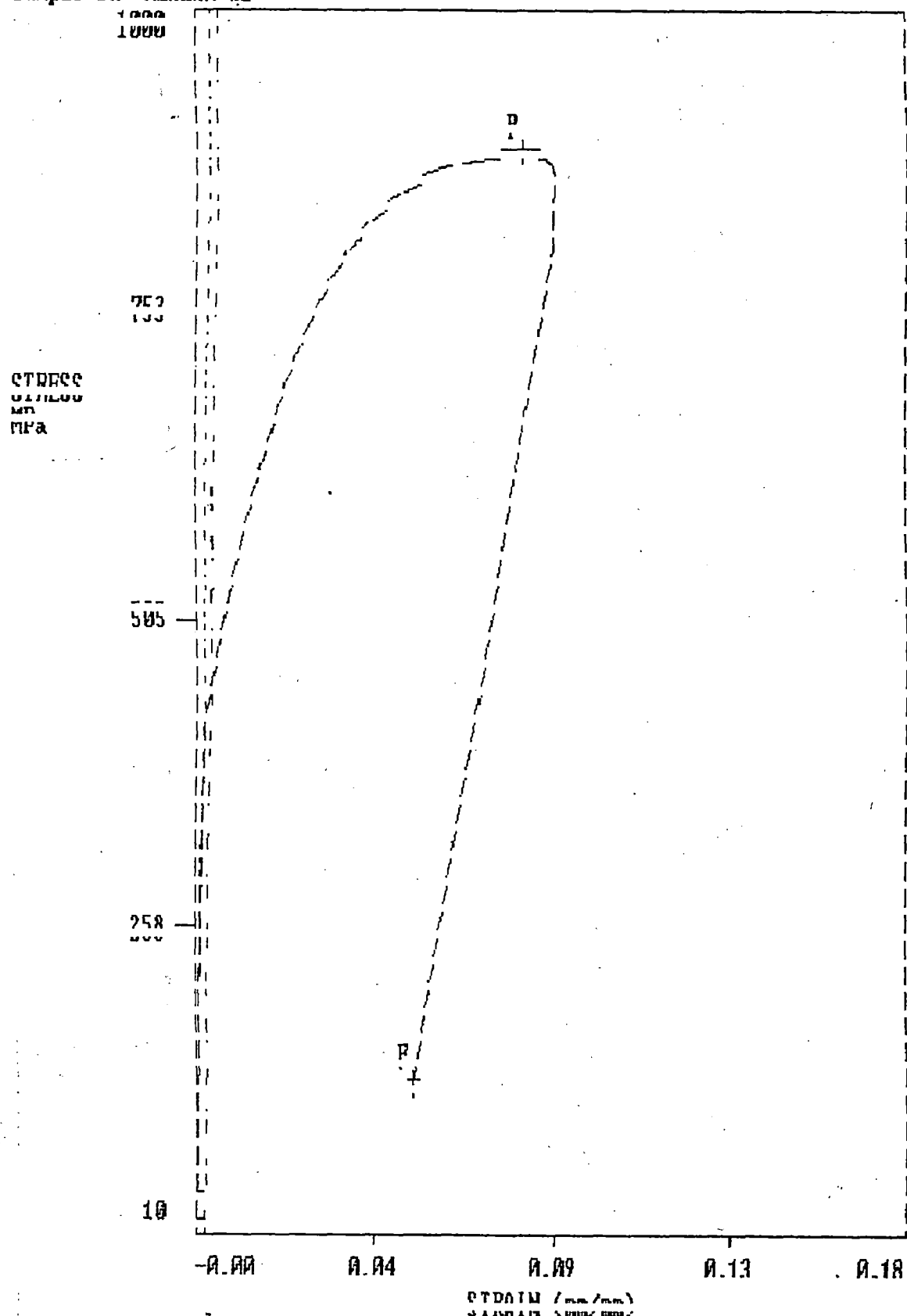


Fig. 4.2 Stress Vs Strain curve of longitudinal specimen (1a)

Sample Id: MEATAM #2

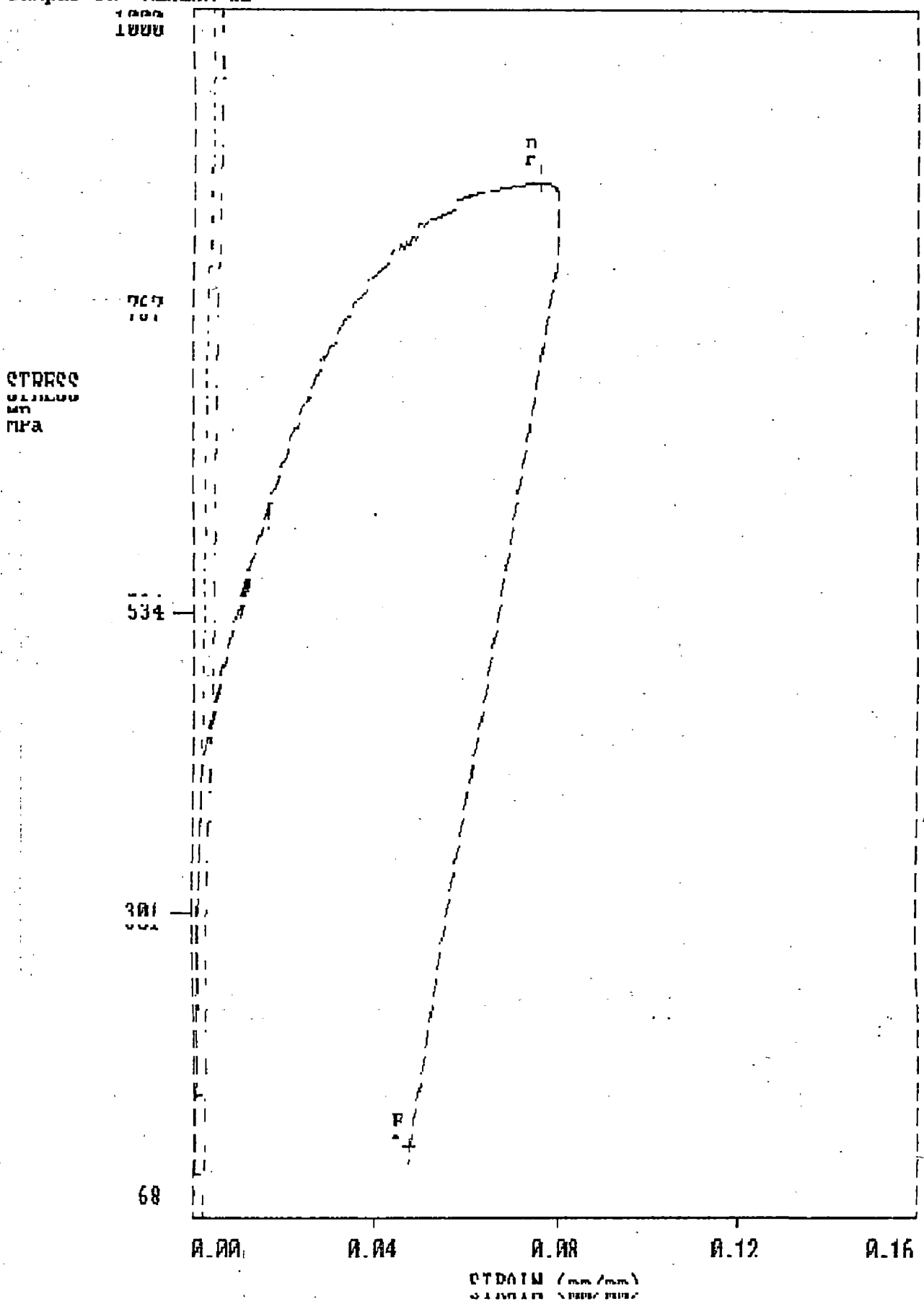


Fig. 4.3 Stress Vs Strain curve of longitudinal specimen (2a)

Sample Id: MRAIAM #3

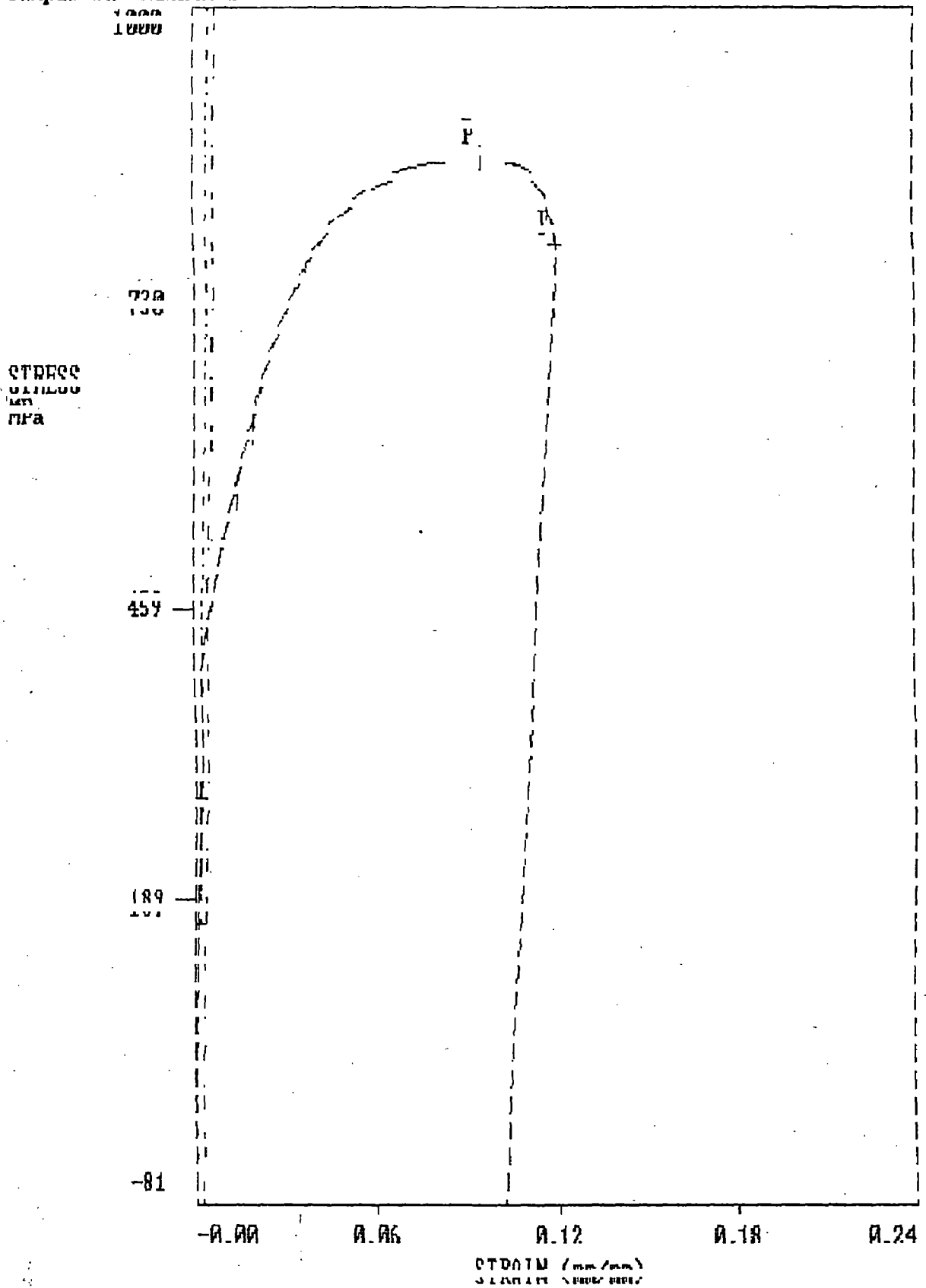


Fig. 4.4 Stress Vs Strain curve of longitudinal specimen (3a)

Sample Id: MEALAM #4

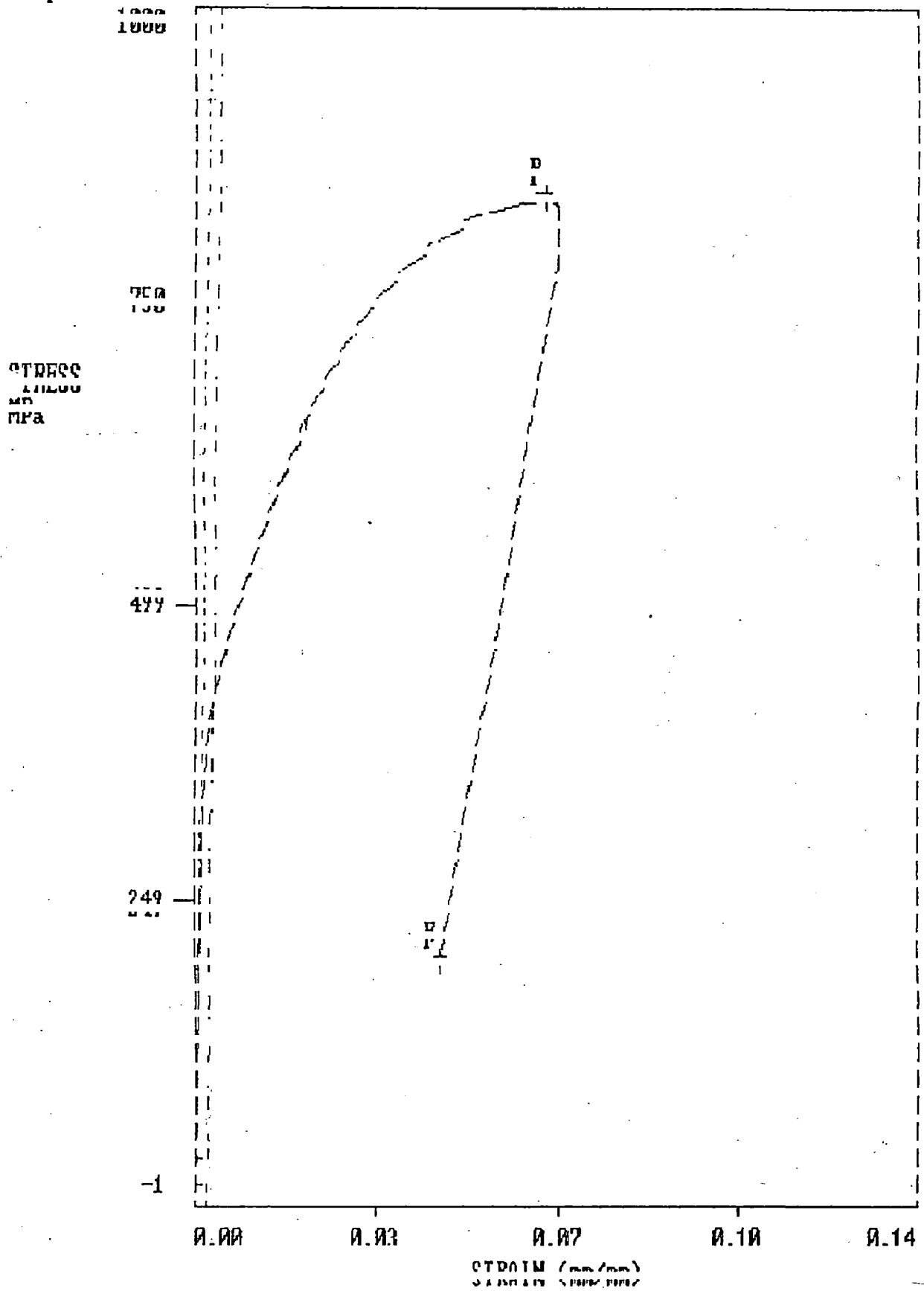


Fig. 4.5 Stress Vs Strain curve of short transverse specimen (2c)

Sample Id: HEALAH #5

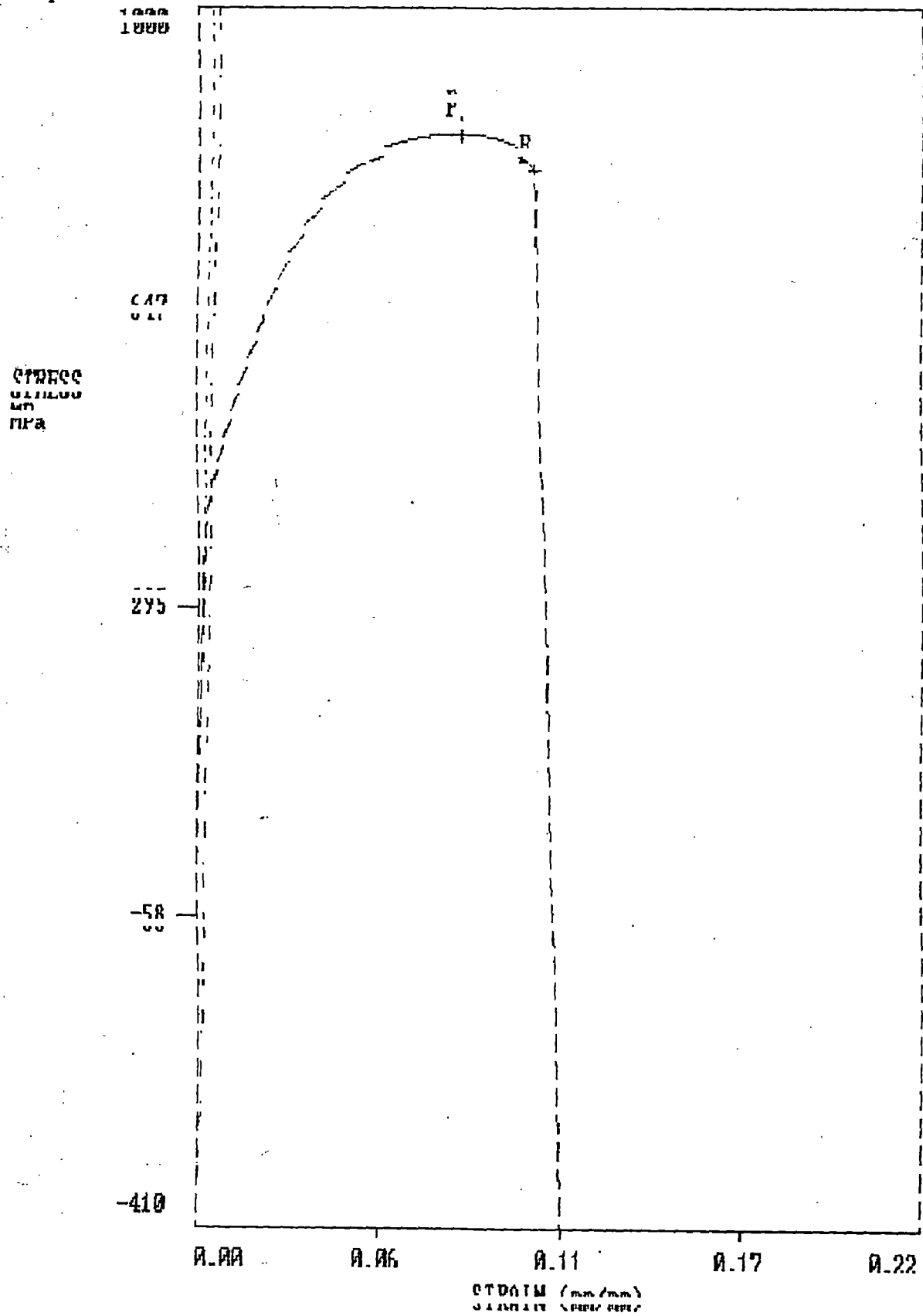


Fig. 4.6 Stress Vs- Strain curve of short transverse specimen (3c)

Sample Id: M021AM #6

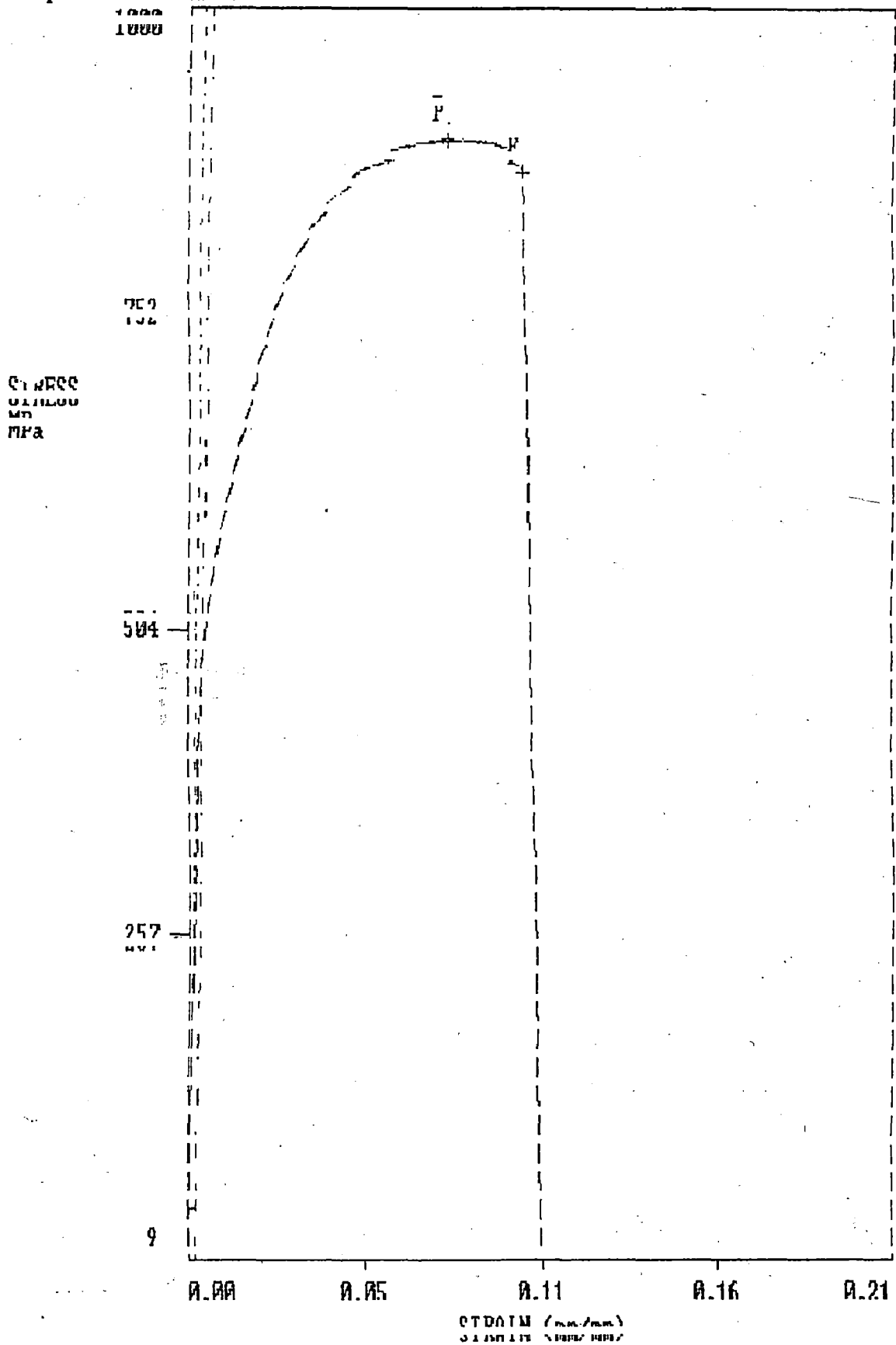


Fig. 4.7 Stress Vs Strain curve of transverse specimen (lb)

Sample Id: HEALAM #7

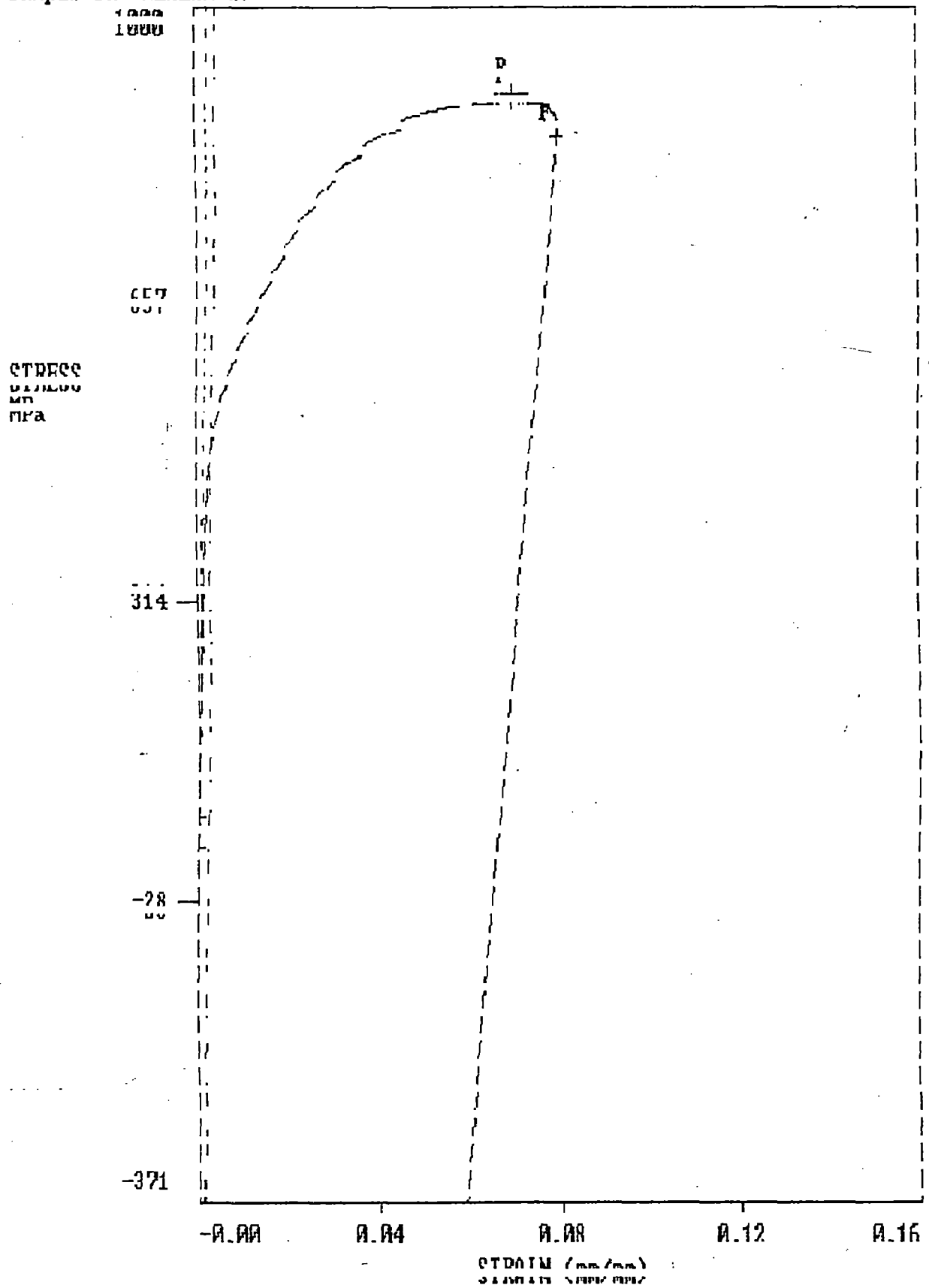


Fig. 4.8 Stress Vs Strain curve of transverse specimen (2b)

Sample Id: M01AM #8

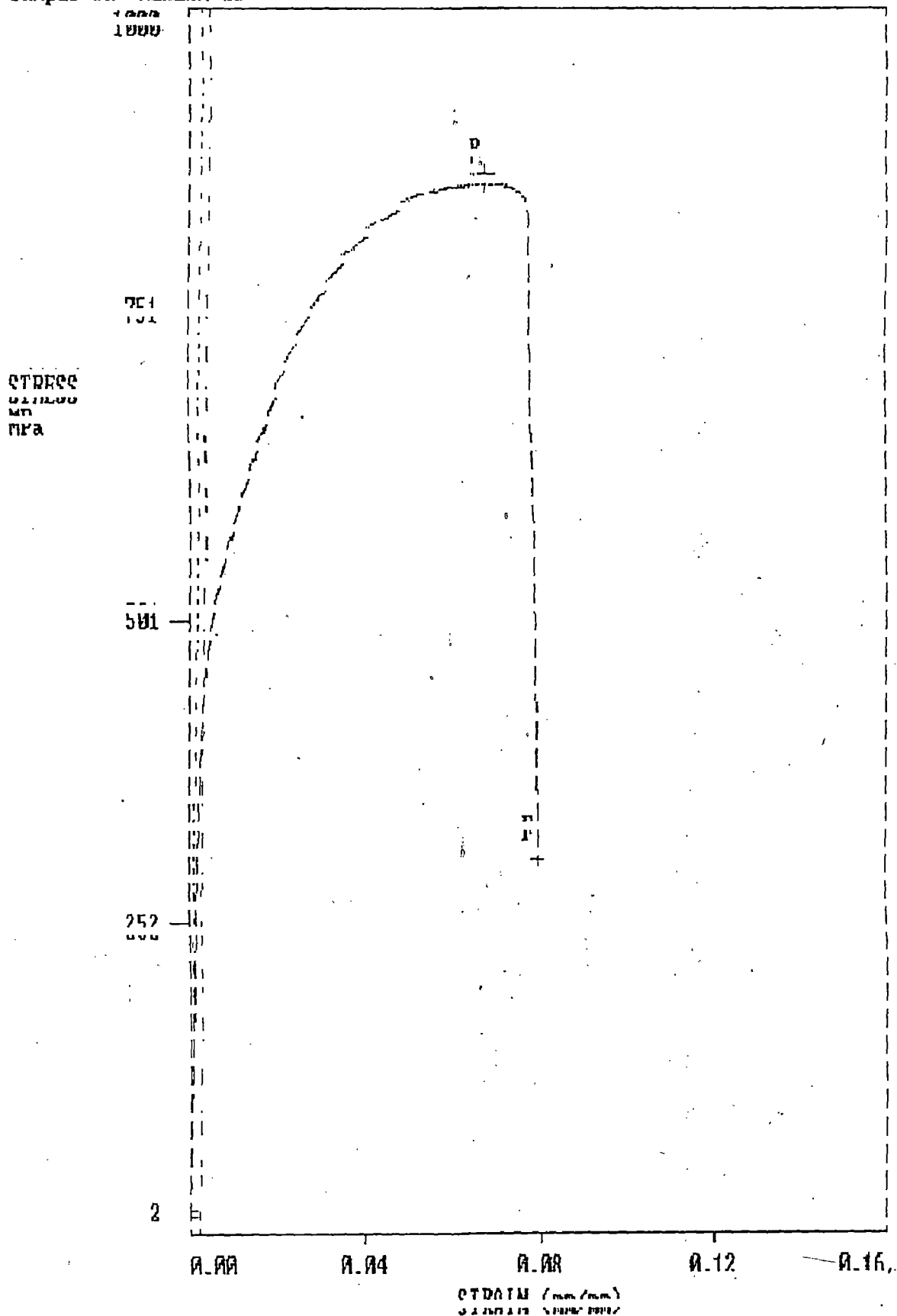


Fig. 4.9 Stress Vs Strain curve of transverse specimen (3b)

POLYNOMIAL da/dN vs. DELTA K

Specimen I.D. : BHH

Job # 12

Test Date : 03-22-1996

Test File : ALAM29

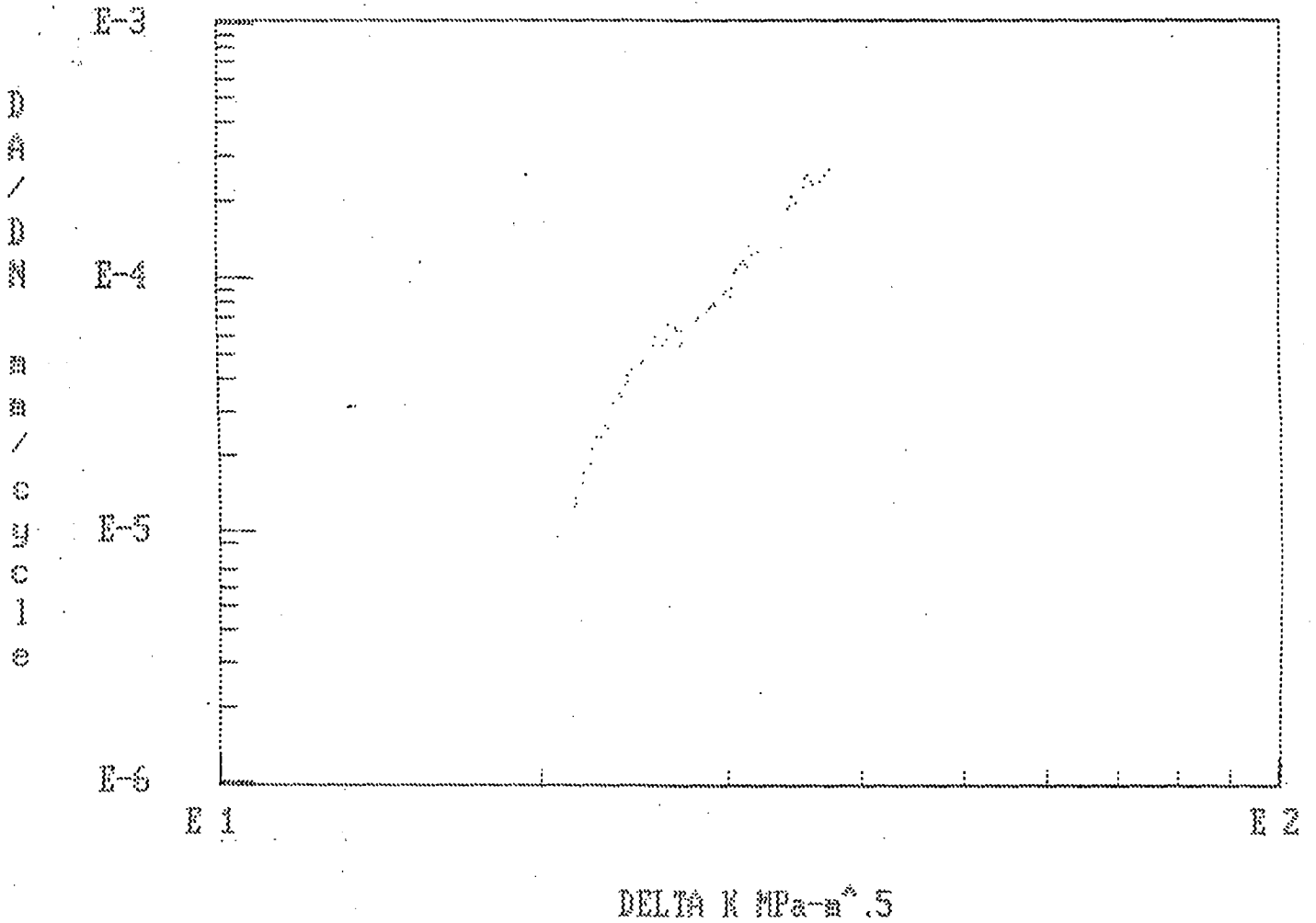


Fig. 4.10 Log da/dN Vs Log (K) curve of specimen - 1.

POLYNOMIAL da/dN vs. DELTA K

Specimen I.D. : RWH

Job # 12

Test Date : 03-16-1996

Test File : ALAM17

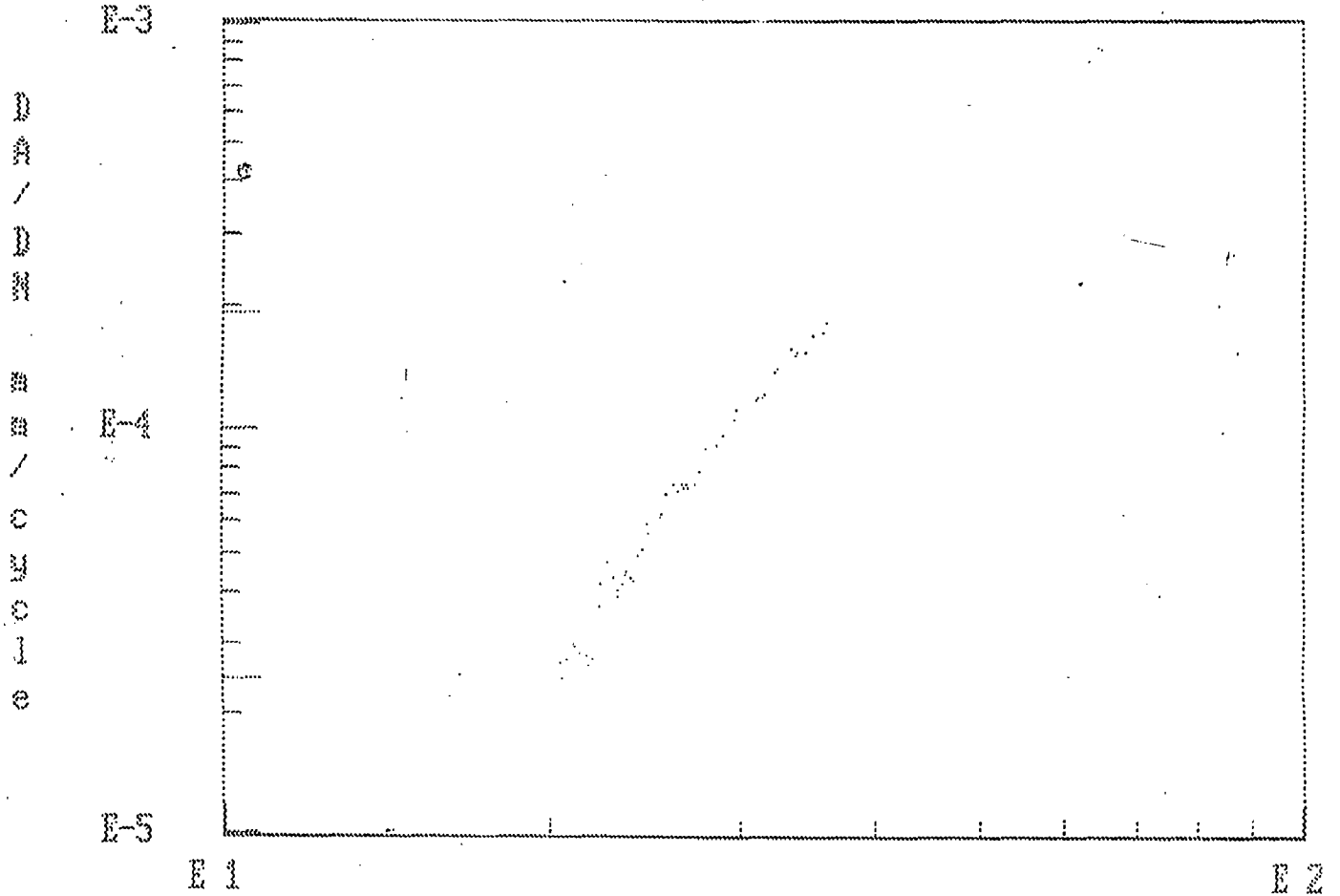


Fig. 4.11 Log da/dN Vs Log (K) curve of specimen - 2

Table 2.1

American Society for Testing and Materials High-Strength
Low -Alloy Structural Steel A 242-63T [5]

1. CHEMICAL REQUIREMENTS			
Carbon, %	0.22 max.	Sulfur, %	0.05 max.
Manganese, %	1.25 max.	Other alloy additions	-
Silicon, %	-		
2. MECHANICAL REQUIREMENTS			
Property	3/4" and under in thickness	Over 3/4" to 3/2" incl. in thickness	Over 3/2" to 4" incl. in thickness
Yield strength, psi	50,000 min.	46,000 min.	42,000 min
Ultimate tensile strength, psi	70,000 min.	67,000 min.	63,000 min.
Elongation, % in 2"	18 min.	19 min.	16 min.
% in 8"	-	-	24 min.



Table 2.2

American Society for Testing and Materials High-Strength
Structural Steel A 440-59T [5]

1. CHEMICAL REQUIREMENTS			
Carbon, %	0.28 max.	Sulfur, %	0.05 max.
Manganese, %	1.10 to 1.60	Phosphorous, %	0.04 max.
Silicon, %	0.30 to 0.33	Copper, %	0.20 min.
2. MECHANICAL REQUIREMENTS			
Property	3/4" and under in thickness	Over 3/4" to 3/2" incl. in thickness	Over 3/2" to 4" incl. in thickness
Yield strength, psi	50,000 min.	46,000 min.	42,000 min
Ultimate tensile strength, psi	70,000 min.	67,000 min.	63,000 min.
Elongation, % in 8" % in 2"	18 min. -	19 min. -	19 min. -

Table 2.3

American Society for Testing and Materials High-Strength
Low-Alloy Structural Manganese-Vanadium Steel A 441-60T [5]

1. CHEMICAL REQUIREMENTS			
Carbon, %	0.22 max.	Vanadium, %	0.02 min.
Manganese, %	1.25 max.	Phosphorous, %	0.04 max.
Silicon, %	0.30 max.	Copper, %	0.20 min.
Sulfur, %	0.05 max.		
2. MECHANICAL REQUIREMENTS			
Property	3/4" and under in thickness	Over 3/4" to 3/2" incl. in thickness	Over 3/2" to 4" incl. in thickness
Yield strength, psi	50,000 min.	46,000 min.	42,000 min
Ultimate tensile strength, psi	70,000 min.	67,000 min.	63,000 min.
Elongation, % in 8"	18 min.	19 min.	19 min.
% in 2"	-	-	24 min.

Table 2.4

Chronological Development of Heat Treatment and Alloying of Rails [15]

PROCESS	REMARKS
1. Heat treatment of Rail Section : To obtain fine pearlite spacings.	Higher working surface hardness but higher costs in reheating.
2. Addition of alloying elements : Standard carbon manganese rail modified with addition of elements such as Cr, Mo, Si, V, Ti and Al.	High strength rails with finer pearlite spacing, expensive alloy addition required.
3. Accelerated cooling after hot : rolling.	Inconsistency in operation.
4. Accelerated cooling during : rolling.	Only head hardened, fine pearlitic structure with good weldability and wear resistance.

Table 2.5

Major Types of Rail Defects and Failure of Rails [15]

1.	Shatter Cracks: hairline cracks in head of rail.	High hydrogen and high Mn/C ratio.	Vacuum treatment, cooling rate $< 8^{\circ}\text{C/h}$, Hydrogen must be < 3 ppm.
2.	Shelling: Horizontal cracks in service	Soft rails, heavy loads results plastic deformation.	Increase hardness and strength of rails.
3.	Transverse fissures: Origin inside of rail head.	Imperfections or large inclusions.	Improve cleanliness of steel.
4.	Transverse Separation: detailed fracture from shelling	Streaks or seams at shelling spots.	Eliminate rolling defects,
5.	Progressive Fracture: Due to compound fissure.	Longitudinal seam, segregation or inclusion.	Improve the cleanliness of steel.
6.	Engine Burn Fracture: Origin a burn due to slipping engine driver.	Initiation of cracks due to brittle martensite phase.	Eliminate slipping engine driver.
7.	Welded Burn Fracture: initiates at resurfaced engine burn.	Thermal cracks due to cooling of resurfaced burn.	Proper cooling of resurfaced burn.
8.	Star cracking: At fish Bolt Holes.	Stress concentration at bolt hole, fatigue crack initiation and propagation.	Reducing the sharpness of holes, use of proper fasteners.

Table 4.1

Chemical Composition of Medium Manganese Rails and Head Hardened Rails

	C (%)	Mn (%)	P (%)	S(%)	Si (%)
Medium Mn Rail	0.5	1.02	0.08	0.05	0.045
Head Hardened Rail	0.55	0.8	0.048	0.044	0.054

Table 4.2

Results of Macro-Hardness Tests

	VHN					
Longitudinal Specimen (along the length)	412	412	396	412	423	396
Transverse Specimen (from the centre to the side)	399	391	371	367	346	330
Short-Transverse Specimen (Top to Bottom)	392	362	329	307	290	270

Table 4.3

Results of Micro-Hardness Tests.

Short-Transverse Specimen	Head	To			Web	
B	348.0	328.5	333.0	293.0	299	294
W	378.0	373.0	395.5	277.5	277.5	272
Transverse Specimen	Centre		To		Side	
B	395.5	397.5	364.5	346.5	337.5	
W	431.5	399.0	373.0	409.0	345.5	
Longitudinal Specimen	Along		The		Length	
B	368		378		330	
W	445		390		368	

Table 4.4

Results of Tensile Tests

Specimen Orientation	Sp.No.	Initial Dia (mm)	Initial X-Area (mm ²)	Final Dia (mm)	Final X-Area (mm ²)	Initial Gauge Length (mm)	Final Gauge Length (mm)	U.S. (MPa)	2% Offset Y.S. (MPa)	R.O.A. (%)	E.A.F. (%)
	1a	7.96	49.76	6.80	36.32	50	56.36	884	468	27.0	12.7
	2a	7.90	49.02	6.84	36.75	50	55.00	867	459	25.0	10.0
	3a	7.94	49.51	6.62	34.42	50	56.7	863	442	30.5	13.0
	1b	5.5	23.76	5.11	20.51	30	33.0	894	474	13.7	10.0
	2b	5.6	24.63	5.11	20.51	30	32.2	898	486	16.7	7.3
	3b	5.1	20.43	4.70	17.35	30	32.5	861	439	15.1	8.0
	1c	7.74	47.05	6.68	35.05	50	53.4	838	425	25.5	6.8
	2c	7.76	47.30	6.73	35.57	50	54.3	837	419	24.8	8.6
	3c	7.98	50.02	7.05	39.04	50	54.8	853	428	22.0	9.6

Table 4.5

Results of Impact Tests (Energy in Joules)

I. Temperature = 0°C				
Specimen Direction	Sp.No.	1	2	3
Longitudinal		7	9	7
Transverse		5	7	6
Short Transverse		7	8	10
II. Temperature = 25°C (Room Temperature)				
Specimen Direction	Sp.No.	1	2	3
Longitudinal		7	8	8
Transverse		7	5	6
Short Transverse		7.5	7.5	5.5
III. Temperature = 70°C				
Specimen Direction	Sp.No.	1	2	3
Longitudinal		11	11	14
Transverse		9	9	8
Short Transverse		9.5	12	10

Table 4.6

Fatigue Crack Growth rate (FCGR) Test Results of Specimen -1

Specimen Parameters:		Pre-crack Control Parameters:	
Specimen width (mm)	60	Pre-crack full scale load (kN)	60
Notch length (mm)	17	Full Scale C.O.D. (mm)	.6
Specimen thickness (mm)	15	Final Kmax. (MPa-m ^{3/2})	20
Modulus of Elasticity (MPa)	210000	Load Reduction step size (%)	20
Yield strength (MPa)	840	Load ratio	.1
		Frequency (Hz)	15
Test Control Parameters:		Calculated Test Results:	
Full scale load (kN)	60	Reduced data type	Polynomial
Full scale C.O.D. (mm)	.6	Highest da/dN in analysis (mm/cycle)	2.71x10 ⁻⁴
Max. Test Load (kN)	14	Lowest da/dN in analysis (mm/cycle)	9.41x10 ⁻⁶
Load ratio	.1	C	1.97x10 ⁻¹²
Frequency (Hz)	15	n	5.21
Final crack length (mm)	30		

Table 4.7

Fatigue Crack Growth rate (FCGR) Test Results of Specimen -2

Specimen Parameters:		Pre-crack Control Parameters:	
Specimen width (mm)	60	Pre-crack full scale load (kN)	60
Notch length (mm)	18	Full Scale C.O.D. (mm)	.6
Specimen thickness (mm)	15	Final Kmax. (MPa-m ^{3/2})	20
Modulus of Elasticity (MPa)	210000	Load Reduction step size (%)	20
Yield strength (MPa)	840	Load ratio	.1
		Frequency (Hz)	15
Test Control Parameters:		Calculated Test Results:	
Full scale load (kN)	60	Reduced data type	Polynomial
Full scale C.O.D. (mm)	.6	Highest da/dN in analysis (mm/cycle)	2.35x10 ⁻⁴
Max. Test Load (kN)	14	Lowest da/dN in analysis (mm/cycle)	1.37x10 ⁻⁴
Load ratio	.1	C	9.98x10 ⁻¹⁰
Frequency (Hz)	15	n	3.41
Final crack length (mm)	32		